**Title**
Nucleic Acid Amplification for Accessible Diagnostics of Chronic and Acute Conditions



**Author**
Hambalek, Jacob Amos

**Publication Date**
2020

Peer reviewed|Thesis/dissertation

UNIVERSITY OF CALIFORNIA

Los Angeles

# Nucleic Acid Amplification for Accessible Diagnostics of Chronic and Acute Conditions

A thesis submitted in partial satisfaction of the requirements for the degree of Master of Science in Bioengineering

by

Jacob Amos Hambalek

2020

ABSTRACT OF THE THESIS

Nucleic Acid Amplification for Accessible Diagnostics of Chronic and Acute Conditions

by

Jacob Amos Hambalek

Master of Science in Bioengineering

University of California, Los Angeles, 2020

Professor Dino Di Carlo, Chair

Nucleic acid amplification is an established strategy for detecting trace amounts of genetic material. Assays employing nucleic acid amplification are prevalent throughout several fields of life science, particularly for diagnostic applications. Advances in access to nucleic acid amplification are necessary to increase its prevalence in laboratory settings and further enable its applicability for point-of-care testing. The work described herein demonstrates several advancements in increasing access to nucleic acid amplification testing. One advancement we demonstrate is an approach for rapid and portable assessment of DNA base methylation, an emerging biomarker correlated to chronic conditions such as cardiovascular disease. This approach incorporates methylation sensitive restriction endonuclease digestion with an isothermal mechanism for nucleic acid

amplification to determine the presence of methylation marks at DNA targets of interest. We additionally demonstrate a platform for digital nucleic acid amplification in microparticle templated water-in-oil emulsions. Utilizing microparticles with cavitary geometries for improved loading of DNA templates, this digital nucleic acid amplification approach requires no specialized equipment and indicates improved reaction efficiency over comparable microparticle platforms. We envision the coalescence of these and other nucleic acid amplification advancements for the democratization of amplification-based technologies to improve the capability and accessibility of nucleic acid diagnostic testing.

The thesis of Jacob Amos Hambalek is approved.

Daniel T. Kamei

Aydogan Ozcan

Dino Di Carlo, Committee Chair

University of California, Los Angeles

2020

**Dedication**

*To my loving support network, without which none of this would have been possible. Y a mis ancestros, que lo nunca imaginían en sus sueños más magicos.*

TABLE OF CONTENTS

**Acknowledgements**

I am incredibly grateful for the phenomenal mentorship from Professor Dino Di Carlo. His insight, vision, and wisdom have cultivated impactful discovery and unrelenting passion from each of his students.

I also consider myself incredibly fortunate to have been a member of such a vibrant and encouraging research community throughout my undergraduate and graduate education. To all past and present members of the Di Carlo Laboratory, especially those I worked with closely, thank you for fostering this nurturing research environment, and for welcoming me into what feels like a second family.

On that note, to my wonderful family: I cannot thank you enough for your eternal support and love. The best dogs, Jack and Brody, have shown me unconditional support through all the ups and downs of growing up. I am thankful for my younger brother and pediatric cancer survivor, Nicolas Frank Hambalek, your courage and brightness inspire us all. I am thankful for my sister, Rebecca Terese Hambalek, your constant support and strength have been a saving grace throughout these very formative years of our lives. I am thankful for my parents, Ruth Quinto and Frank Hambalek, for setting a comprehensive example of perseverance, diligence, and leadership, and for creating opportunities to strive for those qualities in my own endeavors.

I am especially grateful for the one who first inspired my love for learning: my grandmother, Rebecca Patricia Quinto. Your legacy lives on and will live on in all I do.

**Chapter 1** is adapted from the publication (in preparation) authored by: **Jacob Amos Hambalek**[&], Janay Elise Kong[&], Calvin Brown[%], Hector Enrique Munoz[&], Thomas Horn[&], Michael Bogumil[&], Eleni Quick[&], Aydogan Ozcan[%], Dino Di Carlo[&, @]

[&]: Department of Bioengineering, University of California, Los Angeles

[%]: Department of Electrical Engineering, University of California, Los Angeles

[@]: Jonsson Comprehensive Cancer Center, University of California, Los Angeles

For **Chapter 1**, we would additionally like to acknowledge the UCLA 2018-2019 Capstone Design Course students who contributed to this work as part of their Senior Capstone project: Michael Mellody, Akhil Harapanahalli. We would also like to acknowledge the UCLA 2019-2020 Capstone Design Course students who contributed to this work as well: Laila Rad, Zi Wang, Kylee Bauer, Shouzheng Yue, Emily Yan, Nicole Prusty.

**Chapter 2** is adapted from the publication (in preparation) authored by: **Jacob Amos Hambalek**[&], Joe De Rutte[&], Michael Bogumil[&], Ana Gu[&], Jonathan Omens[&], Dino Di Carlo[&,@]

[&]: Department of Bioengineering, University of California, Los Angeles

[@]: Jonsson Comprehensive Cancer Center, University of California, Los Angeles

The author and work were supported in part by the NSF Engineering Research Center for Precise Advanced Technologies and Health Systems for Underserved Populations (PATHS-UP): Award No. 1648451. This work was also supported in part by the UCLA Capstone Course funding through the UCLA Department of Bioengineering.

## Chapter 1: Methylation Sensitive LAMP - Nucleic Acid Methylation Detection Through Loop Mediated Isothermal Amplification

The emergence of epigenetic associated gene regulation and its role in disease has motivated a growing field of epigenetic diagnostics for risk assessment and screening. In particular, irregular cytosine DNA base methylation has been implicated in several diseases, yet the methods for detecting these epigenetic marks are limited to lengthy protocols requiring bulky and costly equipment. We demonstrate a simple workflow for detecting methylated CpG dinucleotides in synthetic and genomic DNA samples using methylation sensitive restriction enzyme digestion followed by loop mediated isothermal amplification. The workflow can be performed in approximately one hour, requiring only a simple heat source. This workflow can provide a foundation for distributable point-of-care testing of DNA methylation levels.

### Graphical Abstract

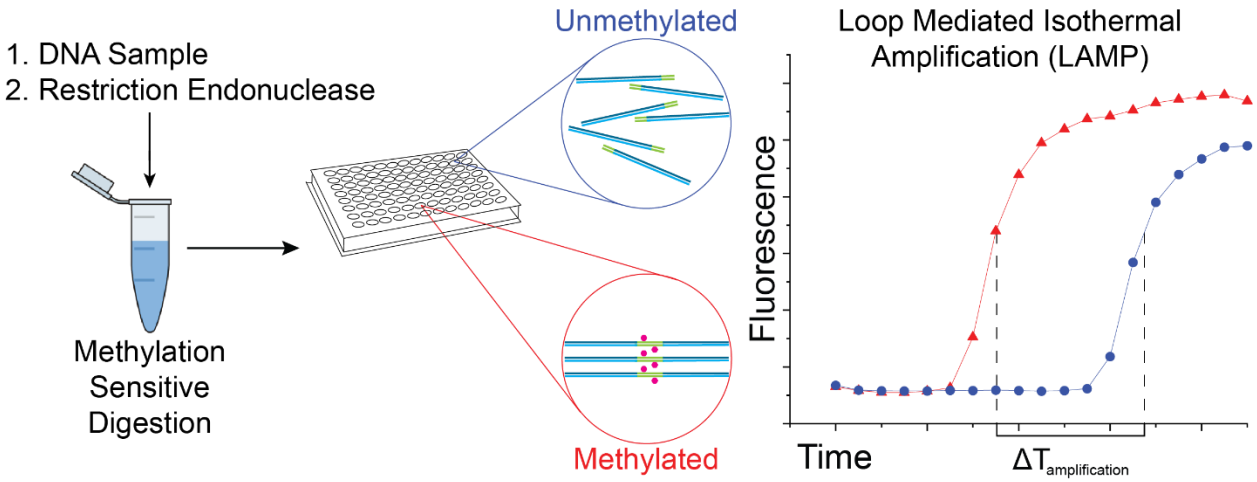


### Introduction

DNA base methylation is a process that regulates gene expression in a locus-dependent manner and can inform on disease processes lacking well-conserved genetic mutations. The presence of methylation within both gene promoter and transcription regions has been inversely correlated with the expression of gene products[1–3]. In mammalian genomes, methylation

primarily occurs at Cytosine bases 5' adjacent to Guanine bases, known as Cytosine-phosphate-Guanine (CpG) dinucleotides[2,4,5].

As DNA methylation levels progressively increase with age in humans, abnormalities in these methylation profiles can induce irregular gene expression, which in turn can lead to disease**.** Aberrant DNA methylation patterns at specific genome locations have been observed in correlation with several diseases, including cardiovascular diseases (CVD) and certain types of cancer[1,4,6,7]. For example, CpG hypermethylation of genes for atherosclerotic protective estrogen receptors *ESR1* and *ESR2* is observed in atherosclerosis patients[8,9]. Genes for angiopoietin growth factors including *ANGPTL2* also undergo distinct CpG hypomethylation in cases of coronary heart disease[7,10]. In cancer, genes responsible for DNA repair, such as *BRCA1*, undergo transcription downregulation through CpG hypermethylation in the promoter[1,5].

In addition to academic study, there has been growing commercial interest in the diagnostic capabilities of DNA methylation through detection of aberrant CpG methylation profiles**.** Recently, the diagnostics company GRAIL reported promising results from clinical trials for early cancer detection via cell free DNA CpG methylation profiling[11,12]. Their platform surveys the methylation profile of several genes associated with tissue-specific cancers, providing a blood based screening tool for over 50 types of cancer[13]. However, the test currently relies on costly next-generation sequencing to perform.

While there is significant work to develop point-of-care (POC) formats for nucleic acid-based diagnostics, there has been minimal demonstration of simplified POC compatible workflows for nucleic acid methylation detection. Nucleic acid amplification is desirable for POC testing of nucleic acid based biomarkers based on its simplicity, speed, and sensitivity[14,15]. For diseases which disproportionately affect underserved communities, DNA methylation may

play a key role in distributable, low cost disease risk stratification[4,16,17]. However, current methods of DNA methylation detection are not suitable for cost-effective distribution in POC, rural, or distributed settings. Common current methods include bisulfite conversion of DNA followed by sequencing or Polymerase Chain Reaction (PCR) amplification based readout[18,19]. Upon treatment with bisulfite, methylated and unmethylated Cytosines are distinguished through the conversion of unmethylated Cytosines into Uracils[20]. Bisulfite conversion and readout protocols require equipment that is confined to central laboratory settings and can take over an hour to several hours in some protocols[21]. Bisulfite conversion is currently not distributable or portable, and therefore is incompatible with POC testing environments. Underserved populations in both rural and urban environments can benefit from POC testing formats, as there can be a lack of infrastructure, such as specialized technicians and fully equipped laboratories and clinics[15,22,23].

To enable the widespread availability of DNA methylation as an emerging POC testing biomarker, new portable and distributable assay formats are needed. Accurate risk assessment for DNA methylation associated diseases in POC environments can enable the expansion and improvement of early disease detection for underserved populations[4,16,18]. A more POC suitable alternative to bisulfite conversion for distinguishing methylated and unmethylated Cytosines is DNA digestion by methylation sensitive restriction endonucleases (MSREs)[24]. Restriction endonucleases are enzymes that cleave single- and double-stranded DNA at short oligonucleotide recognition sites[25]. MSREs do not perform this digestion when their corresponding recognition site is methylated[24,26]. This differentiation between unmethylated and methylated DNA can be detected through DNA amplification, shown previously through post-digestion PCR and electrophoretic separation[21,24,27].

Loop mediated isothermal amplification (LAMP) is an isothermal nucleic acid amplification alternative to PCR with beneficial characteristics for POC use. The isothermal temperature constraint, in contrast with PCR thermal cycling, significantly reduces assay complexity and cost[28–30]. Further, through precise construction of LAMP primer sets of 4-6 oligonucleotide sequences, stem-loop hybridization on initial LAMP products promotes further primer annealing and polymerase extension, thus increasing absolute DNA product yield in comparison to PCR[14,31,32]. The quick reaction times, high product yield, and simple temperature constraints make LAMP a desirable technique for POC diagnostic systems[22,33,34]. LAMP has been used previously for DNA amplification based methylation detection; however, the study utilized bisulfite as the CpG methylation differentiating agent, of which the reaction conditions, such as temperature and time, are unsuitable for POC testing[35].

In this work, we leverage LAMP to develop an assay for DNA methylation detection that is applicable in POC testing environments. Methylation sensitive LAMP (MS-LAMP) determines the presence of CpG methylation through MSRE target digestion followed by LAMP, shown in **Figure 1.1**. This procedure can be performed in ~1 hour isothermally, eliminating complex instrumentation such as a thermal cycler from the workflow. We validated this mechanism upon two DNA targets: λ phage DNA and the promoter of the *BRCA1* gene, both in synthetic form and from long genomic DNA obtained from breast cancer cell lines. The hypermethylation of the *BRCA1* promoter is associated with aggressive subtypes of breast cancer[36].

**Materials and Methods**

*DNA oligos and target sequences:* λ phage DNA was purchased from Thermo Fisher Scientific (Waltham, MA, USA). The linear 600 bp segment of the *BRCA1* promoter was purchased from Life Technologies (Carlsbad, CA, USA). All primers were ordered through

Invitrogen Custom Oligos (Carlsbad, CA, USA). Primer sequences are available in **Supplemental Table 1.1**.

*DNA Methylation and Target Preparation:* All DNA targets were methylated with CpG Methyltransferase M.SssI kit (Thermo Scientific) according to manufacturer's protocols. Targets used for "Unmethylated" experimental conditions were prepared with all components of the M.SssI kit except for the M.SsiI enzyme. Fully methylated DNA samples were used as LAMP targets for "CpG Methylated" experimental conditions. For experiments investigating DNA targets with fractional CpG methylation, aliquots of fully unmethylated λ DNA and fully methylated λ DNA were combined in controlled ratios.

*Restriction Enzyme Digestion*: SsiI restriction enzyme kits were ordered from Thermo Scientific. DNA targets at concentrations of 0.045 µg/µL and 1.5 ng/µL for λ DNA and *BRCA1*, respectively, were digested with 0.33 units/µL of the restriction enzyme corresponding to the restriction site(s) within each target sequence according to the manufacturer's "PCR product" protocol (6.7% v/v digestion buffer) as all DNA targets were linear.

*Agarose Gel Electrophoresis:* 1% w/v Agarose gels were prepared in TBE buffer (89 mM Tris, 89 mM Boric Acid, 2 mM EDTA) with 0.01% v/v SYBR Green I nucleic acid stain (Sigma Aldrich, St. Louis, MO, USA). Gels were loaded into a Mini GT Electrophoresis Cell and with voltage supplied by the PowerPac Power Supply (Bio-Rad, Hercules, CA, USA). Electrophoresis was performed at 95 V for 1:10 and viewed via UV illumination. 100 base pair ladders were loaded for DNA strand length reference (Thermo Scientific).

*LAMP Components and Conditions:* All salts were purchased from Sigma Aldrich (St. Louis, MO, USA). LAMP reactions were performed at pH 8.8 and buffered with 20 mM Tris-HCl, 10 mM KCl, 10 mM $(NH_4)_2SO_4$, and 8 mM $MgSO_4$. 1M Betaine (Sigma Aldrich) was

added for melt temperature uniformity between the AT and GC rich regions of the template DNA. The reaction mixture also consisted of 1.6 mM of dNTPs (Invitrogen, Carlsbad, CA, USA), 320 U/mL Bst 2.0 WarmStart DNA Polymerase (New England Biolabs, Ipswich, MA, USA), 1.25 μM Evagreen intercalating dye (Biotium, Hayward, CA, USA), and 120 μM Hydroxynaphthol Blue (Sigma Aldrich, St. Louis, MO, USA). LAMP primers at concentrations of 1.6 μM FIP and BIP, 0.2 μM F3 and B3, and 0.4 μM Loop F and Loop B were present in the LAMP reaction mixture. 0 DNA (ultrapure DI water) was used as the negative control, and varying levels of target DNA, methylated or unmethylated and either restriction enzyme treated or untreated, were used as the various DNA positive conditions. All reactions were run in replicates of 3 to 5 in 50 μL volumes on a 96-well plate (Corning, Corning, NY, USA) at 65 °C for up to 2 hours. Kinetic fluorescence values at 485 nm excitation and 535 nm emission wavelengths were obtained using the Biotek Cytation 5 Plate Reader (Winooski, VT, USA) for runtimes between 1-2 hours.

*Genomic DNA Extraction for* BRCA1 *targeting:* MCF7 and HCC38 breast cancer cell lines were cultured in DMEM (Gibco, Waltham, MA, USA) with 10% FBS (Gibco) and 1% Penicillin-Streptomycin (Gibco). Cells were cultured in T-25 flasks to confluency, and DNA was extracted using the PureLink Genomic DNA Mini Kit (Invitrogen) according to manufacturer's protocol.

*Statistical Analysis:* As amplification delay is a key parameter in determining DNA methylation level in this mechanism, $EC_{50}$ time values from sigmoidal fitting provide a higher degree of accuracy in quantifying amplification time compared to a simple threshold time. Text file exports from the Cytation 5 Plate Reader were analyzed with a custom R script (available from GitLab upon request). Briefly, data from each well in which a reaction took place was fit

with a 4-parameter sigmoidal function: Slope, Lower, Upper, and $EC_{50}$. As $EC_{50}$ represents the halfway value between upper and lower fluorescence values, we considered the time associated with this $EC_{50}$ value as the effective amplification time. Each amplification time was then grouped by experimental condition. A single factor ANOVA was performed to confirm group rejection of the null hypothesis. Post Hoc T-tests assuming unequal variance were then performed, and p-values were adjusted with the Holm-Bonferroni correction for multiple comparisons. The T-tests were one-tailed as we hypothesized later amplification times in populations with lower degrees of CpG methylation.

**Results**

In MS-LAMP, LAMP primers were designed to incorporate MSRE digestion sites both within and between primer binding regions. **Supplemental Figure 1.1** shows the sequences targeted in this work, highlighting the LAMP primer regions and MSRE restriction sites. As a first step, DNA samples were incubated with the MSRE and thus digested at each corresponding restriction site containing no methylated CpG dinucleotides, as shown in **Figure 1.1a**. The samples were then amplified via LAMP with DNA target concentration uniformity among all samples.

Following DNA template restriction digestion, exponential amplification was delayed. The proposed mechanism of methylation detection through MS-LAMP is described in **Figure 1.1.** Template digestion within an inner primer binding region creates a 5’ overhang upon primer annealing, shown in **Figure 1.1b**. As polymerase can only polymerize DNA from 3’ overhangs, digestion at that location is expected to disable amplification from initiating at that site, thus delaying the exponential stage of amplification. In primer designs where the inner primer binding region remain intact on the reverse complementary strand relative to the amplicon, polymerase

extension initiated from that site is expected to proceed as normal. This likely leads to the formation of stem-loops on one side of the amplicon only, referred to herein as "half-dumbbells", as shown in **Figure 1.1c**. These half-dumbbell conformations may also be obtained upon template digestion between the forward and reverse primer binding regions, as both regions must be present within the same DNA strand to achieve the full dumbbell amplification product conformation.

The DNA intercalating fluorescent dye Evagreen was used to measure DNA amplification yield through fluorescence intensity[37]. The addition of the sequestering dye Hydroxynaphthol Blue (HNB) further increased fluorescence sensitivity of Evagreen through reduction of background fluorescence, enhanced signal stability, and a greater signal-to-noise ratio[38]. This increase in sensitivity and baseline stability further motivated the use of fluorescence for amplification detection as opposed to other less sensitive optical sensing modalities.

We first developed an MS-LAMP protocol for λ phage DNA, differentiating between unmethylated and in vitro methylated samples. The MSRE SsiI was selected because its recognition site was present within the forward inner primer binding region of a primer set previously used in targeting λ phage DNA[38]. **Supplemental Figure 1.1** shows the full λ phage DNA primer regions and SsiI restriction sites. The template strand separates into two DNA strands at the site where the Forward Inner Primer (FIP) initially binds, thus interfering with polymerase extension through the expected creation of a 3' overhang upon FIP binding, as shown in **Figure 1.1b**. This interference of amplification was confirmed experimentally, shown in **Figure 1.2a**, with an observed time to amplification delay of approximately 20 minutes in unmethylated digested λ DNA. An observed ~10-fold change in fluorescence above baseline enabled clear characterization of DNA amplification indicated by fluorescent intercalating dye.

Non-MSRE treated controls shown in **Figure 1.2a** confirmed that CpG methylation itself had no impact on amplification kinetics.

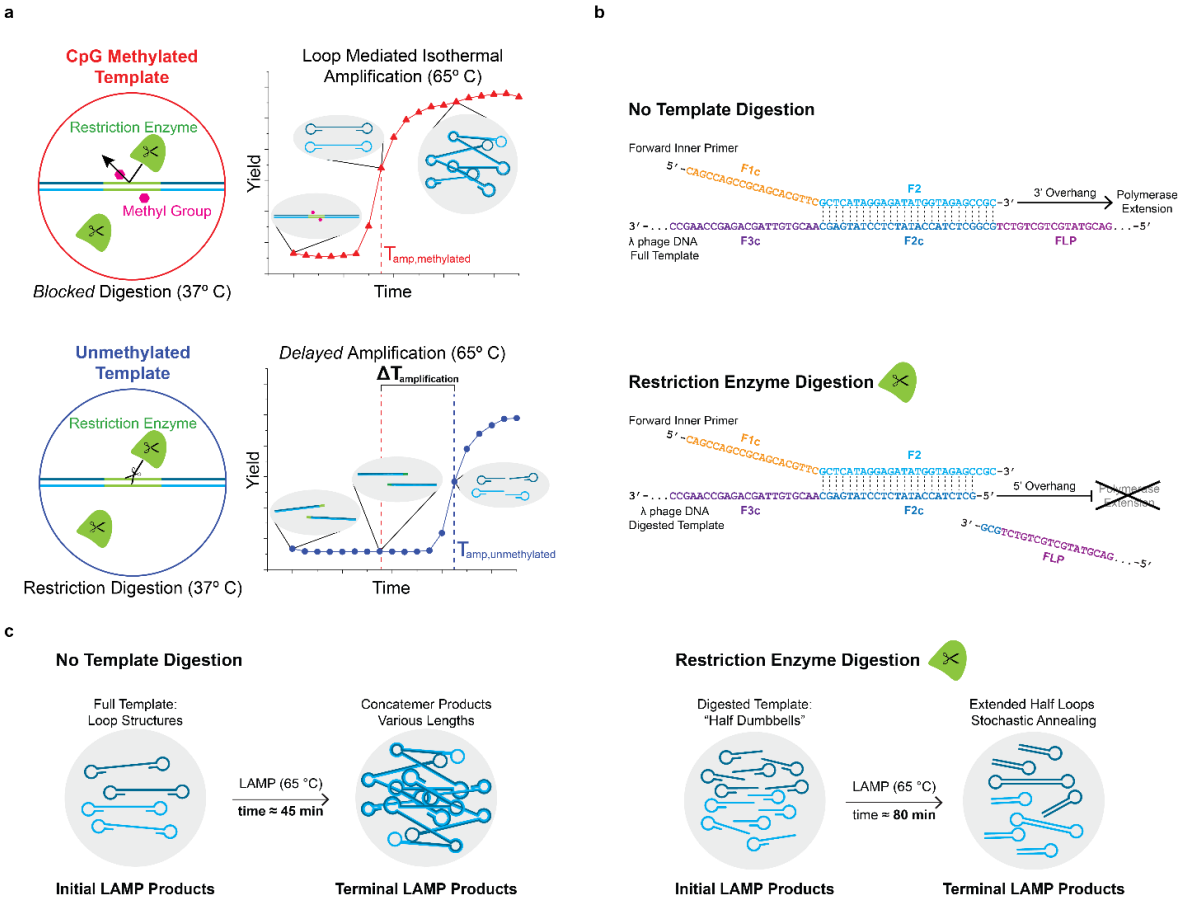


***Figure 1.1: Restriction Digestion of LAMP template induces amplification delay via "Half Dumbbell" Stem-Loop Conformations***. ***A***. *When unmethylated, the DNA template is cleaved at the site of MSRE recognition, separating sections of the amplicon from one another and leading to a delay in amplification. Methylated CpG dinucleotides at these sites block MSRE function and maintain the full size of the LAMP template, thus having no impact on amplification. Hypothesized amplification products differ in conformation, thus inducing a change in amplification time (ΔT) through decreased frequency of concatemer formation in digested targets.* ***B***. *LAMP inner primer binding for λ phage DNA, selected as a proof of concept target.*

*Template digestion by SsiI MSRE occurs at the 3' end of the F2 inner primer binding region. Upon binding of the inner primer, a 5' overhang occurs when the template is digested, and therefore is not recognized by the polymerase as an extension site.* ***C.*** *Evolution of LAMP product conformations as amplification proceeds. Full dumbbell stem-loop conformations induce continuous template amplification and the formation of concatemer amplicon repeats on the same DNA strand. Upon digestion of the template either within a primer binding region or within the amplicon, single stem-loop "half dumbbells" are formed as the forward and backward primer regions are separated from each other. Later annealing of half dumbbells into full stem-loop products is hypothesized to be mediated by single stranded complementary "randomers" added by polymerase at the 3' end of half dumbbells.*

To obtain optimal methylation sensitive restriction digestion, we tuned the restriction enzyme conditions for digestion. The level of digestion was highly dependent on concentrations of both restriction enzyme and DNA target. Restriction enzymes were examined at varying component concentrations. **Supplemental Figure 1.2** shows the optimization of concentrations of each component used for subsequent experiments. Adhering to manufacturer-recommended enzyme concentrations ensured optimal digestion, as increasing the restriction enzyme concentration over the manufacturer recommended protocol led to a reduction in digestion efficiency.

Once the MS-LAMP workflow was developed for λ phage DNA, we expanded our testing library to other DNA targets with disease relevance. A 600 base pair segment of the *BRCA1* promoter was synthesized and targeted with MS-LAMP. The methylation level in this region of the gene promoter is associated with breast cancer, and has been shown to affect the potency of various chemotherapeutics in tumor reduction[1,5,6]. The same MSRE, SsiI, was selected for this

target, however, the LAMP primer set generated for this target did not contain the restriction site within any inner or outer primer binding region, shown in **Supplemental Figure 1.1**. Rather, multiple SsiI restriction sites were located in the amplicon between the primer binding regions. Upon digestion, the forward and reverse primer binding regions are separated from each other into independent DNA strands, and thus are expected to yield the half-dumbbell conformation upon initial product generation, as hypothesized for λ phage DNA.

Kinetic measurements of amplification of methylated and unmethylated DNA targets show distinct differences in amplification time upon digestion with SsiI. Similar to the delay observed in λ phage DNA, an approximate 20-minute delay in amplification was observed in the unmethylated *BRCA1* DNA targets upon MSRE digestion, shown in **Figure 1.2b**. DNA target concentration was kept identical across all methylation and restriction enzyme conditions. The sample concentration for both targets shown in **Figure 1.2**, on the order of $10^4$ copies/μL, was informed by reported yields of common genomic DNA extraction kits[39,40]. Validating the MS-LAMP workflow in this range of target concentration enabled future assessment of CpG methylation in genomic DNA with MS-LAMP. Agarose gel electrophoresis confirmed the prevention of digestion as a result of CpG methylation. **Figure 1.2c** and **Figure 1.2d** indicate that both λ phage and synthesized *BRCA1* DNA strand size was only significantly altered when unmethylated and treated with MSREs, confirming that methylated DNA strands block digestion by SsiI.

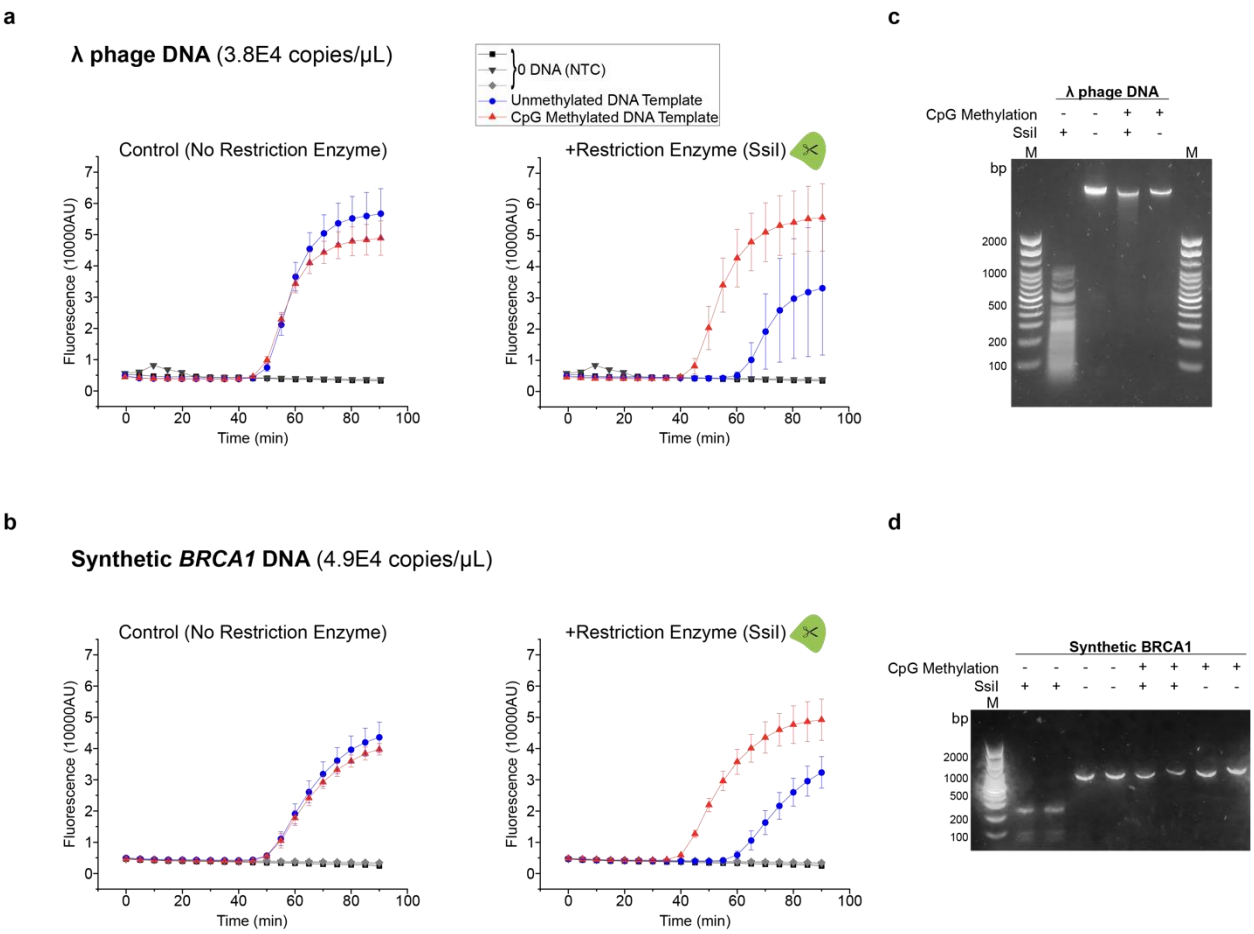


***Figure 1.2: Delay in DNA Amplification as a Result of Template Digestion by Restriction Enzymes. A,B.*** *LAMP kinetic fluorescence measurements taken at 5-minute intervals targeting unmethylated and methylated (A) λ DNA and (B) synthetic BRCA1 DNA, respectively. A distinguishable delay in amplification occurs in the unmethylated target treated with MSRE. Non MSRE treated controls show no impact on amplification as a result of CpG methylation.* ***C,D.*** *Agarose gel electrophoresis images of post-SsiI digestion (C) λ DNA and (D) synthetic BRCA1 LAMP templates pre-amplification to determine post-digestion template strand length. Template size was only altered in unmethylated DNA strands treated with MSRE. CpG methylation of the target strands thus prevents digestion of the strand by MSRE SsiI.*

We observed significant methylation dependent changes in the amplification speed for both targets. Sigmoidal curve fitting of kinetic amplification data has been previously shown to provide high resolution quantification of amplification time[41]**.** Using a four-parameter sigmoidal fit, the midpoint of the exponential amplification regime, known as the $EC_{50}$ value, was selected as the effective point at which amplification was confirmed. The time value associated with these $EC_{50}$ fluorescence values was selected as the time to amplification, shown in **Figure 1.3a**. **Figure 1.3b** demonstrates the significantly distinct delay in amplification time in digested LAMP targets (p-value < 0.001 for λ phage DNA, p-value < 0.01 for *BRCA1*).

Difference in amplification time values between unmethylated and methylated targets informed the selection of an assay endpoint time to ensure the presence of amplification was associated with methylated DNA samples. Amplification time values for λ phage and *BRCA1* DNA targets informed selection of a preferred endpoint time between 60-70 minutes for both sequences, indicated as horizontal dashed lines in **Figure 1.3b**. Endpoint times facilitate a simpler assay design requiring only one fluorescence measurement, where obtaining a clear fluorescent signal would indicate the presence of CpG methylation in the LAMP target. This design can further enable wide distribution of CpG methylation screening, as it could be conducted outside of laboratory settings using only a heat source and mobile fluorescence reader.

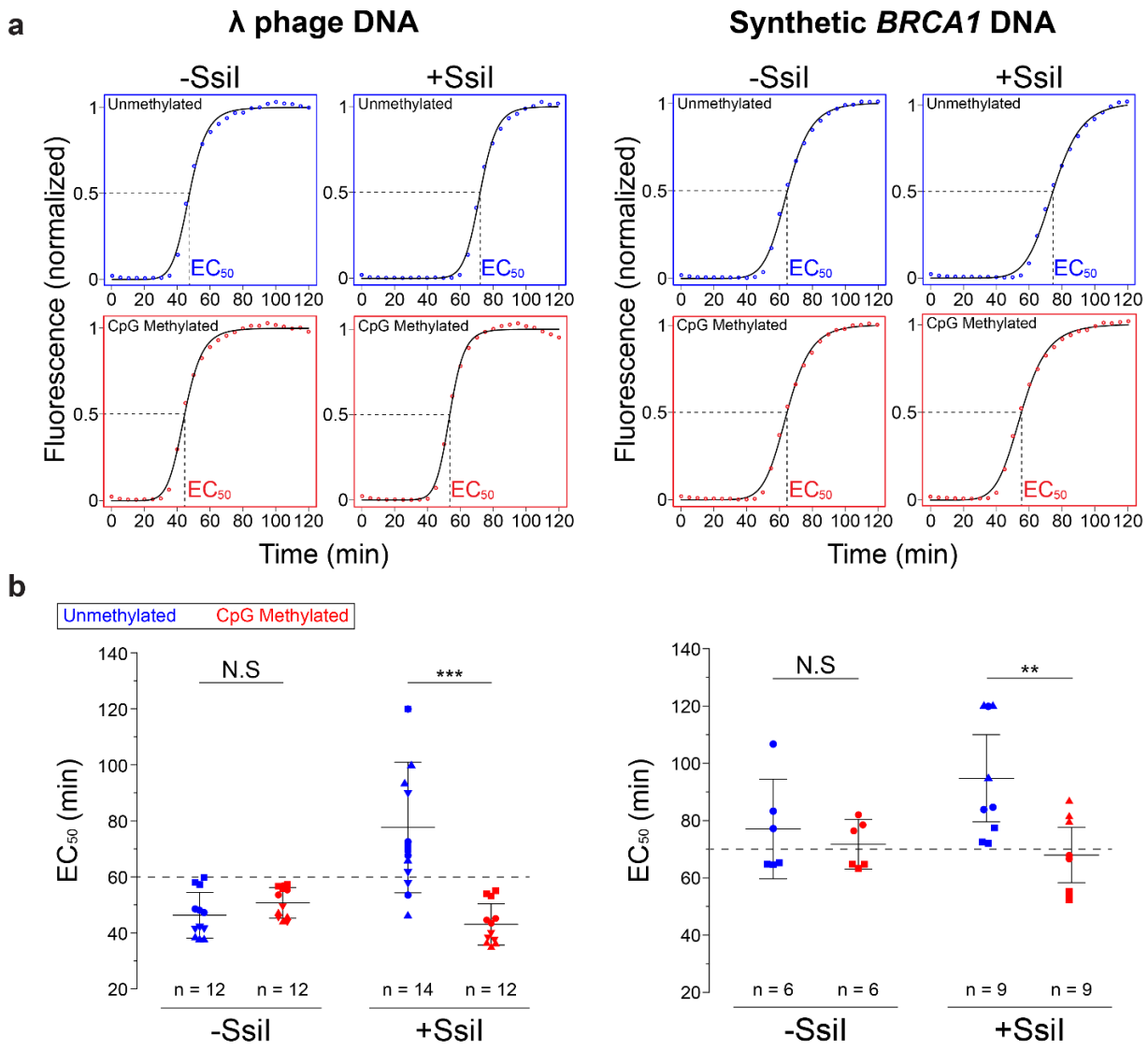


***Figure 1.3: Sigmoidal curve fit quantifies amplification rate through $EC_{50}$ time values. A.*** *Raw fluorescence values taken at 5-minute intervals for LAMP targeting λ DNA and synthetic BRCA1 DNA with sigmoid curves fit to the data. The timepoint associated with the $EC_{50}$, the point at which fluorescence is halfway between the upper and lower sigmoid bounds, was selected as the effective amplification time for each reaction. As amplification was delayed in unmethylated digested DNA targets, a later $EC_{50}$ time was calculated in those conditions.* ***B.*** *Scatter plot of $EC_{50}$ times over several experiment trials with an illustrative threshold endpoint time indicated by dashed lines. Significant ($p<0.001$ for λ DNA, $p<0.01$ for BRCA1 DNA) difference in*

*amplification time between unmethylated and methylated DNA targets was observed upon treatment with SsiI. Mean line and standard deviation error bars are shown for each DNA target condition. Different symbols indicate separate days upon which the experiments were performed.*

As DNA methylation levels also progressively increase in healthy individuals, clinically relevant methylation profiling will not consist solely of detecting the presence of methylation, rather the frequency of CpG methylation as a percentage of DNA at a particular locus**.** Differences in amplification speed between samples containing different ratios of methylated vs. unmethylated template copies are shown in **Figure 1.4b**. The amplification speed increased as the ratio of methylated DNA increased, consistent with the observed decrease in amplification speed in fully unmethylated in comparison to fully methylated DNA targets shown in **Figure 1.3**. Agarose gel electrophoresis, shown in **Figure 1.4a**, indicates an increasing quantity of full size λ phage DNA template in the sample as the ratio of methylated DNA increases, indicating a greater ratio of methylated λ phage DNA copies resistant to endonuclease digestion.

Statistical significance between the amplification of DNA samples with varying ratios of methylated DNA was observable**.** Here we used a t-test accounting for unequal variance. The Holm-Bonferroni correction was applied to p-value significance cutoffs to account for multiple comparisons. Statistically distinct amplification times are observed in samples with at least two orders of magnitude difference in methylation level. Samples with less than 1% methylation display significantly slower amplification kinetics than samples with methylation ratios above 11%. Within these two groups, however, there was little statistically significant difference in amplification time.

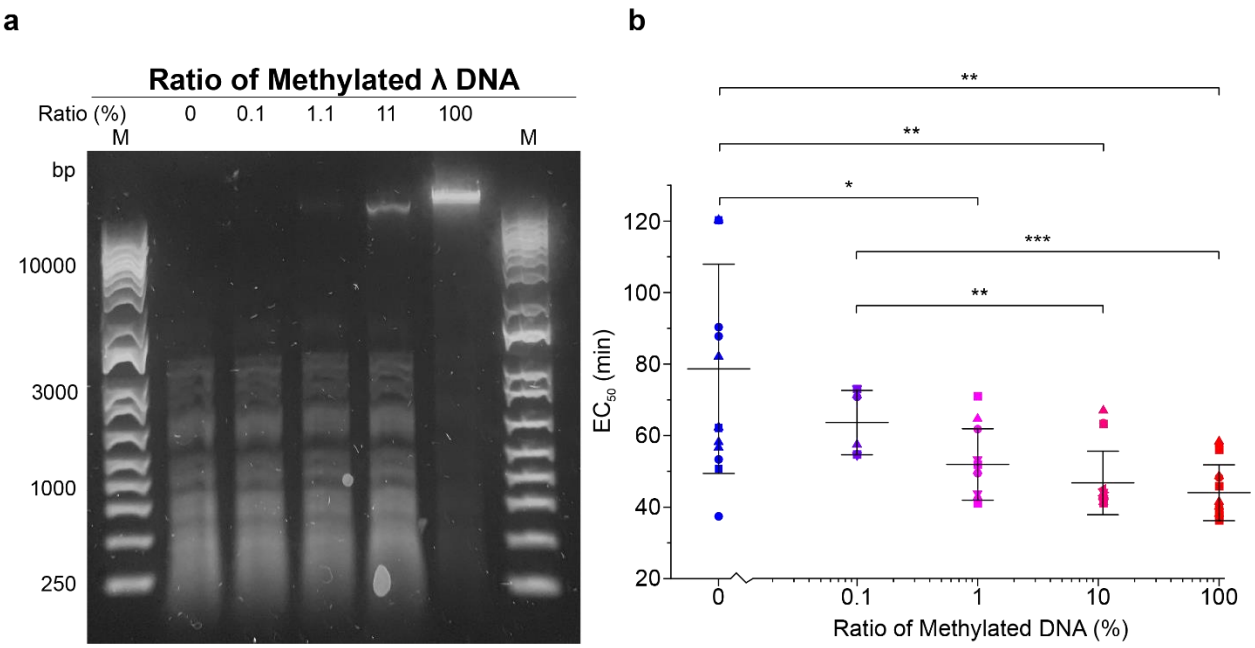


***Figure 1.4: Ratio of CpG methylated vs. unmethylated templates affects LAMP amplification time. A.*** *Agarose gel electrophoresis image of post-SsiI digestion λ phage DNA samples with varying ratios of CpG methylated to unmethylated template copies. Increase in methylated template copy ratio results in increased presence of full length λ DNA.* ***B.*** *$EC_{50}$ time values for samples with varying ratios of template with CpG methylation. Mean line and standard deviation error bars are shown for each DNA target condition. Different symbols indicate different days upon which the experiments were performed. *: $p<0.05$, **: $p<0.01$, ***: $p<0.001$ with adjustment using the Holm-Bonferroni correction.*

Observing methylation dependent amplification differential for *BRCA1* in a synthetized target inspired investigation of *BRCA1* MS-LAMP amplification differential in genomic sourced *BRCA1* DNA samples. As *BRCA1* promoter methylation has been associated with varying breast cancer phenotypes, two breast cancer cell lines with differing *BRCA1* promoter methylation, MCF7 and HCC38, were selected as gDNA sources for MS-LAMP[36]. MCF7 cells show near complete demethylation throughout the *BRCA1* promoter, and HCC38 shows CpG methylation

levels above 90% at the CpG sites targeted within the MS-LAMP *BRCA1* primer set, as shown in **Figure 1.5a**[42,43]. Upon digestion with SsiI, a methylation dependent amplification differential was observed between gDNA samples obtained from MCF7 and HCC38, as observed through kinetic fluorescence measurements shown in **Figure 1.5b**.

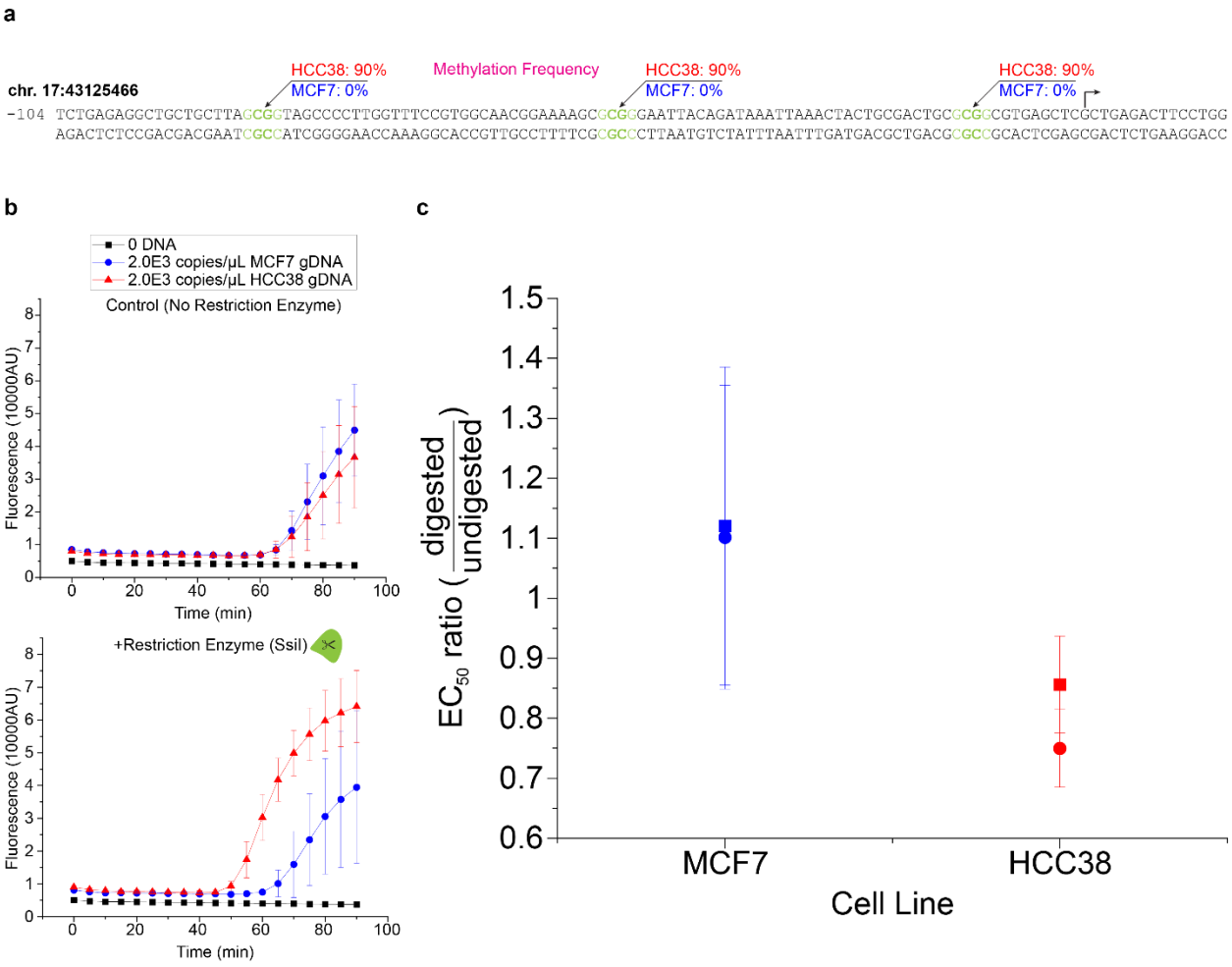


***Figure 1.5: BRCA1 amplification differential observed in breast cancer cell lines of differing CpG methylation. A.*** *Region of the* BRCA1 *promoter targeted with MS-LAMP. The three CpGs assessed exhibit drastically different CpG methylation frequency in cell lines MCF7 and HCC38, with MCF7 exhibiting near complete demethylation and HCC38 exhibiting near complete methylation at these CpG sites* ***B.*** *Kinetic fluorescence measurements targeting* BRCA1 *in MCF7 and HCC38 sourced DNA samples. These genomic DNA samples were targeted with the*

*same LAMP primers utilized for the synthetic* BRCA1 *MS-LAMP targeting.* ***C.*** *$EC_{50}$ amplification time ratios for MCF7 and HCC38 genomic DNA samples. Ratio of digested target amplification times to undigested control sample amplification times demonstrates the amplification delay as a result of target demethylation while accounting for amplification kinetic improvement as a result of digestion at sites outside of the LAMP amplicon. Error bars indicate the propagated error associated with the standard deviation of replicates for each condition. Different shaped symbols indicate the average $EC_{50}$ ratio for one experiment (3 replicates for each condition).*

We took the ratio of digested sample $EC_{50}$ amplification times to undigested control sample amplification times to most accurately quantify the delay in amplification observed in MCF7 extracted DNA samples in comparison to those extracted from HCC38. As several SsiI restriction sites exist throughout the genome, the length of the DNA segment with the LAMP target was expected to decrease upon SsiI digestion. Decreased DNA segment length has been shown to improve the kinetics of DNA amplification[44,45]. This effect was observed in the amplification of HCC38 sourced DNA samples, where the CpG methylation within the amplicon preserves the full length of the target but digestion at other sites likely decreases the length of the DNA segment containing the target. For MCF7, the calculated amplification time ratio was greater than 1, indicating that the delay associated with digesting the LAMP target itself contributes more to the amplification kinetics than the segment length decrease effect.

**Discussion**

Including MSRE digestion, we demonstrate a total MS-LAMP workflow time of 70-80 minutes. The most accelerated protocols for MS-PCR workflows are reported to be completed in a minimum of 101 minutes: 40 minutes for bisulfite conversion, 61 minutes for PCR[21,46]. The

time advantage and less stringent temperature requirements of MS-LAMP improve the POC applicability of this mechanism in contrast to MS-PCR. Further primer optimization may lead to a shorter workflow time due to reduction in time to amplification, as some reported LAMP reactions are detectable after 10-20 minutes[47,48].

Template digestion within a LAMP inner primer binding region likely prevents polymerase extension at that binding site**.** Exponential amplification is therefore hindered likely through the presence of a 5' overhang upon primer annealing to a template digested within the binding region. The half-dumbbell stem loop conformations of initial products of digested templates limit the number of polymerase extension sites, reducing the frequency of long concatemer product generation, in contrast to full dumbbell conformations. Though the location of restriction sites differs between the λ phage and synthesized *BRCA1* target sequences, the half-dumbbell conformation is likely formed in both targets, as the forward and reverse primer regions are separated into two distinct DNA strands in both cases.

The mechanism of delay in amplification may result from multiple factors. The delayed exponential amplification of digested DNA targets may occur via annealing of half-dumbbell products into full dumbbell conformations**.** Recent studies have demonstrated pairwise stem-loop annealing via single stranded "randomers" added to the 3' end of amplified products by polymerase[47]. The resultant amplification from these products, sometimes even occurring in negative controls, is observed later than on target amplification, indicating a significant time period required for complementary randomer annealing. It is possible this could incur full dumbbell LAMP products from digested templates via complementary randomer mediated half-dumbbell annealing. Upon annealing of complementary randomers, a 3' overhang is generated, which can then be recognized by polymerase as an extension site for amplification.

Additionally, the digestion within the inner primer binding region may reduce the primer binding affinity at that site, further delaying amplification**.** As the primer binding region is separated into two different strands of DNA, there is a truncation of complementary bases for primer annealing. This truncation leads to a decrease in melting temperature of the primer binding region, indicating reduced affinity of that sequence to its complement and therefore slower binding kinetics[44]. A melting temperature between 60 °C and 65 °C for F2 has been shown to be ideal for LAMP[28]. A change in melting temperature to 55.3 °C was calculated for the F2 region of the FIP for the λ phage DNA target , shown in **Supplemental Table 1.2**.

Amplification in unmethylated samples may also occur as a result of imperfect enzymatic digestion of each template copy. Even at 99% digestion efficiency, several DNA strands containing the full template length would remain in the DNA sample. As LAMP is particularly sensitive even at femtomolar target concentrations, template amplification, albeit delayed, may occur through the presence of these complete template strands at a lower effective concentration. However, the electrophoresis results shown in **Figure 1.2b** indicate that the MSRE digestion efficiency is sufficient to prevent observation of fluorescent signal on the gel from undigested target strands in unmethylated samples.

Selection of an assay endpoint time further facilitates the qualitative detection of DNA methylation in a POC setting**.** An endpoint between the amplification times for unmethylated and methylated samples thus connects any measured amplification signal qualitatively with the presence of CpG methylation within the DNA sample, enabling a use of a simple fluorimeter to assess DNA methylation level. This fluorescence reader could be portable and handheld to further enable POC applications for this workflow. This endpoint time selection, shown in **Figure 1.3b**, was adjusted between the λ phage and synthesized *BRCA1* target sequences, as the

amplification kinetics for each target varied based on binding affinity of the respective primer sets for each target. This parameter must also be optimized for each target using real time amplification measurement before using solely endpoint fluorescence measurements.

Physiological understanding of CpG methylation indicates that like cell types maintain highly conserved CpG methylation profiles within their epigenome[2,3,27]. In our investigation of partial DNA methylation levels shown in **Figure 1.4**, experimental procedures entailed combining fully CpG methylated DNA with fully unmethylated DNA. The CpG methylation percentage of each sample was determined by the ratios in which the methylated and unmethylated DNA are combined. While this sample preparation method has been utilized in previous in vitro studies, CpG methylation percentage in biological samples, in contrast, corresponds to the fraction of CpG sites within a single DNA strand that are methylated[49]. This physiological CpG methylation profile is difficult to achieve via in vitro enzymatic methylation, and thus motivates further study with genomic cell and clinically sourced samples.

When assessing the methylation level of genomic DNA samples with MS-LAMP, the ratio of digested to undigested sample amplification times provides a clearer metric for determining methylation level than amplification time alone**.** This ratio accounts for the effects on reaction kinetics as a result of digestion that occurs outside of the LAMP target. The amplification speed increase as a result of this digestion competes with the amplification delay caused by digestion within the LAMP target yet **Figure 1.5c** shows that the target digestion-induced delay in unmethylated samples is the dominant effect. These effects must be well characterized in real time for genomic DNA MS-LAMP targets before distribution as an endpoint assay. Additionally, undigested sample controls may be necessary for the POC workflows for some MS-LAMP targets where the segment length effect is more pronounced.

Further generalization of this mechanism to other DNA targets whose methylation level is indicative of disease will further demonstrate the applicability of this workflow in serving as a POC DNA methylation assay. Primer sets and MSRE selection, informed by the interrelation between primer binding regions and restriction sites, must be individually optimized for each target. LAMP primer generation software such as Eiken Chemical PrimerExplorer can be utilized to generate a library of primer sets for each desired target, which can then be cross referenced with various MSREs, each with a corresponding restriction site. Real time amplification measurements are thus needed to confirm robust amplification and sensitivity to restriction digestion by one or more selected MSREs.

Improvements in digestion efficiency through a multiplicity of restriction sites may enable further applicability to a larger library of compatible DNA targets, including genome regions where disease phenotype is dependent on partial rather than complete CpG methylation. This can be achieved through digestion protocols using multiple MSREs, an established strategy for homology directed repair for in vitro gene editing[50]. Additional prospects of furthering modularity in template digestion includes investigation of a CpG methylation sensitive CRISPR/Cas9 cleavage system, where digestion sites are determined by a readily synthesized guide RNA. Further investigation of mobile readout for digital LAMP formats is also necessary to enable to the POC applicability of a digital nucleic acid amplification test.

A high degree of variance in amplification time was observed, particularly within the unmethylated digested DNA target population, which can be overcome by running multiple parallel reactions or in a digital format. Due to this high variance and the stochastic nature of LAMP, multiple simultaneous amplification reactions may yield a more accurate quantification of methylation level[47]. Digital platforms, such as droplet digital LAMP (dLAMP), may yield a

more quantitative measure of amplification and have been shown to enable counting of methylated DNA templates[49,51–53]. Digital quantification can directly identify ratios of CpG methylation on a DNA template region with the increased resolution necessary for further use as a diagnostic biomarker. This quantification may improve upon the amplification results obtained from varying CpG methylation ratios in analog assay format, shown in **Figure 1.4**. As DNA methylation associated disease epigenotypes often differ in ratios of CpG methylation rather than complete methylation or demethylation, direct quantification of DNA methylation ratios through a digital assay format ensures more accurate disease profiling[6,49,54].

The ability to isolate a DNA target of interest from patient tissue impacts the nucleic acids that are practically targeted. Genomic DNA extractions are currently difficult to achieve in resource-limited settings. This motivates further investigation of targets derived from cell free DNA (cfDNA) in human serum, as well as DNA from readily obtainable cell types, such as platelets, as DNA methylation associated biomarkers[6,18,21,55]. Mitochondrial DNA samples from platelets, of which the CpG methylation level of several genes has been implicated in various forms of CVD, are readily obtainable via low speed centrifugation and/or filtering of whole blood[56,57]. These particular DNA samples can enable a full POC assay workflow for CpG methylation, from sample acquisition and isolation to amplification results via fluorescence readout.

**Conclusion**

We have demonstrated a mechanism for detecting DNA CpG methylation that is compatible with resource limited testing environments. Without the need for complex and lengthy bisulfite conversion and PCR based protocols, the simple MS-LAMP workflow should

facilitate the application of DNA methylation-based risk assessment and/or diagnostics for several diseases.

The recent excitement of CpG methylation as a diagnostic target, as evidenced by growing commercial platforms for DNA methylation-based cancer screening, may be furthered by simple and low-cost workflows such as MS-LAMP. The MS-LAMP workflow may further support additional diagnostic research in discovering additional CpG methylation associated biomarkers for disease. For example, the workflow could be employed for rapid epigenomic phenotyping of various cell types, such as assessing *FOXP3* demethylation to identify regulatory T-cells[58]. The MS-LAMP workflow therefore may serve as a simple yet versatile tool in the emerging field of DNA methylation research and diagnostics in both field and laboratory settings.

**Appendix A: Supplemental Information for Chapter 1**

***Supplemental Table 1.1: Primer sequences for each LAMP target****. All sequences are provided in 5' to 3' orientation.*

**ST1.1A: λ phage DNA**

| | |
|---|---|
| FIP | **CAGCCAGCCGCAGCACGTTCGCTCATAGGAGATATGGTAGAGCCGC** |
| BIP | **GAGAGAATTTGTACCACCTCCCACCGGGCACATAGCAGTCCTAGGGACAGT** |
| F3 | **GGCTTGGCTCTGCTAACACGTT** |
| B3 | **GGACGTTTGTAATGTCCGCTCC** |
| LoopF | **CTGCATACGACGTGTCT** |
| LoopB | **ACCATCTATGACTGTACGCC** |

**ST1.1B: *BRCA1* DNA**

| | |
|---|---|
| FIP | **GACAGGCTGTGGGGTTTCTCTCCCGGGACTCTACTACCTTT** |
| BIP | **GTAATTCCCGCGCTTTTCCGTCTGTCCCTCCCATCCTCTG** |
| F3 | **GAAATCCACTCTCCCACGCC** |
| B3 | **CAATCCAGAGCCCCGAGAGA** |
| LoopF | **TCAGGAGGCCTTCACCCTC** |
| LoopB | **GGAAACCAAGGGGCTACCG** |

***Supplemental Table 1.2: Melting temperature difference after digestion within the primer binding region****. All melting temperature values were calculated using OligoCalc (Kibbe, W.A)*

*open source software. The "Basic" melting temperature values are reported herein after adjustment for FIP primer concentration and monovalent cation salt concentration (1.6 µM and 10 mM respectively). Decrease in melting temperature indicates reduced affinity for the oligonucleotide primer and its target within the DNA template.*

| Full λ phage F2 (°C) | Digested λ phage F2 (°C) | Difference (°C) |
|---|---|---|
| 61.1 | 55.3 | **-5.8** |

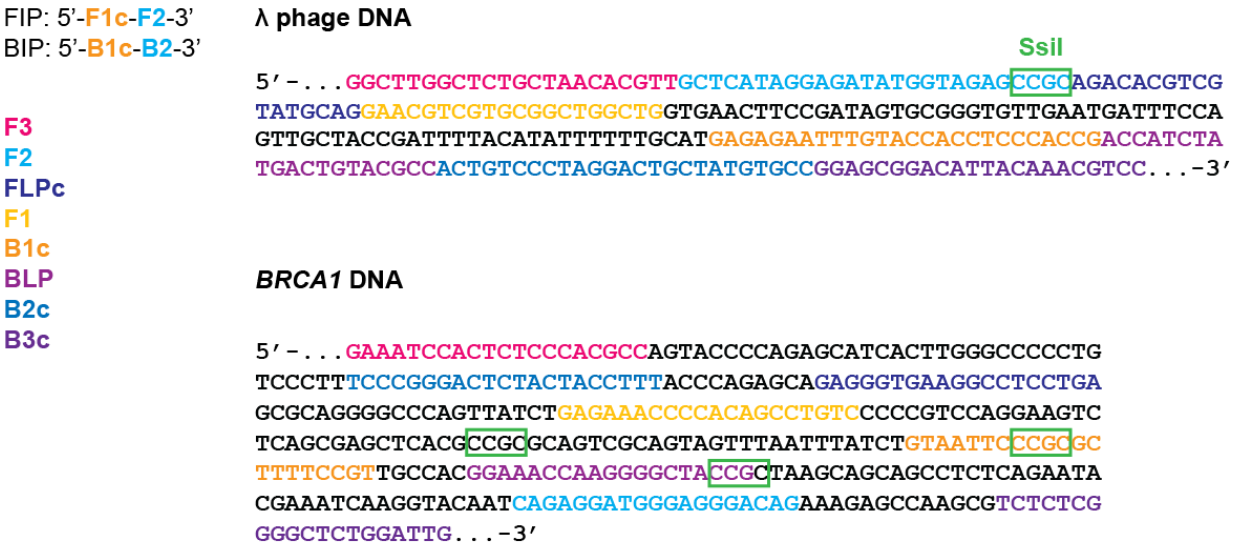


***Supplemental Figure 1.1: LAMP Primer Sets and Restriction Sites.*** *Sequences of both λ phage and BRCA1 MS-LAMP DNA targets, with restriction digestion sites highlighted in green boxes. Restriction digestion, which induces the separation of forward and backward primer binding regions onto two separate strands, is likely responsible for the delay in amplification. The two targets demonstrate two different methods of inducing amplification delay, as digestion occurs within the forward inner primer binding region of λ phage DNA but between the forward and reverse inner primer binding regions in the BRCA1 target.*

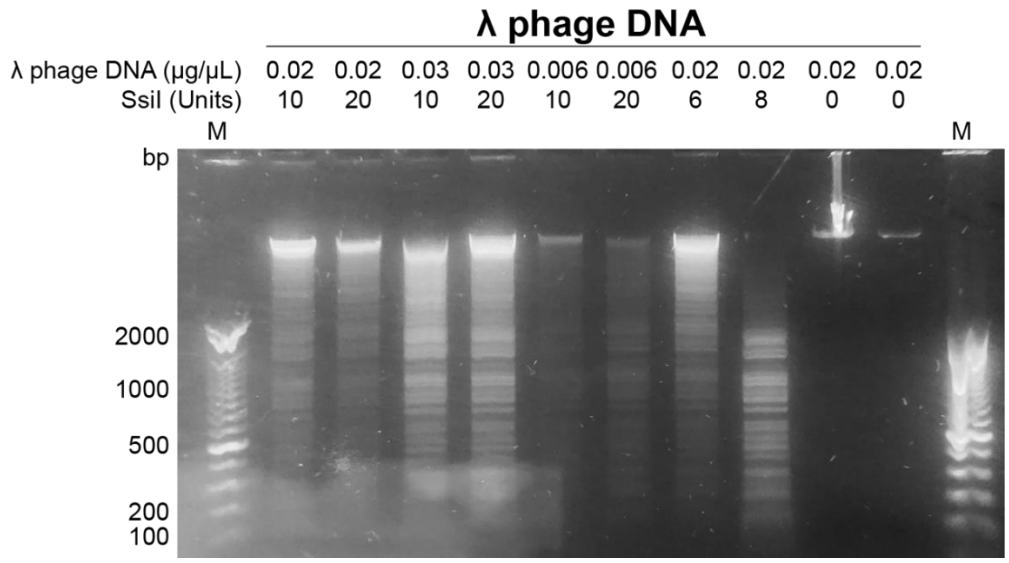


***Supplemental Figure 1.2: Restriction Enzyme Digestion Optimization.*** *Agarose gel electrophoresis demonstrating digestion efficiency of various restriction enzyme and DNA concentrations. The condition (8 units SsiI) which yielded the absence of a band at the height of the undigested DNA, indicated highly efficient digestion, was selected for the remainder of digestion protocols.*

## Chapter 2: Democratized Digital Polymerase Chain Reaction in Uniform Cavitary Microparticle Templated Emulsions

Advances in target quantification for nucleic acid amplification can expand the utilization of our DNA methylation assay described in **Chapter 1** as well as that of assays already established, such as those for diagnosis of acute infections. The quantitative capabilities of nucleic acid amplification are greatly enhanced when conducted in a digital platform, in which single nucleic acid entities are isolated into individual partitions and the ratio of amplified/non-amplified partitions indicate the quantity of nucleic acid in the sample. Reaction partition generation via hydrogel templated emulsions is a promising new approach to digital assays, as the materials required are more readily accessible than specialized and costly partition generation platforms. We demonstrate preliminary data toward a democratized platform for digital polymerase chain reaction (dPCR) using hydrogel templated water-in-oil emulsions. We utilized microparticles with open cavities, which we theorize can increase dPCR reaction quantitative accuracy in comparison to conventional spherical microparticles. The use of cavitary microparticle platforms for dPCR can further increase access to quantitative nucleic acid amplification assays.

### Introduction

Digital assays enhance the quantitative capabilities of diagnostic tests through lower limits of detection and absolute quantification of target analytes[59]. Digital polymerase chain reaction (dPCR) has been shown to have several quantitative advantages over real-time PCR (rtPCR), including improved copy number quantification, precision, and robustness[60–62]. Upstream bisulfite conversion of DNA has also enabled very precise and sensitive detection of methylated DNA loci with dPCR[53,63].

Implementation of a digital format for PCR requires fractionation of assay components into nanoscale partitions. Upon tuning the size and quantity of these partitions to the estimated DNA sample concentration, each of these partitions is considered to contain either one or zero nucleic acid entities[51,64]. After the assay is completed, quantification of DNA in the loaded sample is accomplished through analysis of the ratio of "on" partitions, which contain a DNA entity and elicit an amplification response, to "off" partitions, in which there is no entity and no DNA amplification occurs[65].

Several platforms for performing dPCR have been established, many with key drawbacks. Numerous commercial dPCR systems are predicated upon microfluidic approaches for creating water-in-oil droplet emulsions[65]. While accurate and precise, the cost and benchtop footprint of these platforms is often prohibitive for those outside of specialized digital assay research settings. There are other chip-based commercial platforms that achieve sample partitioning via hydrophilic/hydrophobic patterning, yet several researchers report difficulty in reliably loading assay reagents using these platforms and recommend additional equipment to ensure proper loading[48,66].

There are recently demonstrated platforms for achieving dPCR sample partitioning that utilize hydrogel microparticles to serve as emulsion templates without the need for precise microfluidic droplet generators[67,68]. However, the hydrogel polymer matrix of the microparticles is exclusionary to large macromolecular PCR reagents, such as DNA polymerase and template DNA. Thus, the spherical geometry of these microparticles yields only a thin shell of reaction volume between the emulsion interface and the exterior of the microparticle for polymerization of DNA. This limited reaction volume can hinder the volume-dependent DNA entity Poisson loading, therefore reducing quantitative accuracy and dynamic range[62,69]. The fluctuations in size

of this thin shell may additionally induce high reaction volume variability, which has been shown to reduce the precision and quantitative accuracy of dPCR assays[70,71]. Thus, the current inaccessibility for efficient yet cost-effective dPCR platforms limits the broader utilization of dPCR, motivating new platforms to address this gap in access.

In this work, we demonstrate preliminary data for digital PCR in uniform hydrogel templated emulsions. We used hydrogel microparticles fabricated using aqueous two-phase separation to yield an open cavity within the microparticle. When emulsified, these cavitary microparticles reduce the microparticle-macromolecule exclusion effects as observed in spherical microparticles. The microparticle templated emulsions are generated using simple pipetting and benchtop centrifugation: laboratory equipment that is readily available in most research environments. Upon emulsification, PCR was performed using a standard PCR thermal cycler and subsequently imaged using fluorescence microscopy, with fluorescent intercalating dye indicating the presence or absence of amplification in each partition.

**Materials and Methods**

*Microparticle fabrication*: The cavity geometry microparticles were fabricated as described previously[72]. The microparticles are composed of 10 kDa 4-arm PEG-norbornene (Creative PEGworks) and crosslinked under ultraviolet light using Lithium phenyl-2,4,6-trimethylbenzoylphosphinate (Sigma-Aldrich, St. Louis, MO, USA). The cavitary geometry is achieved using aqueous two-phase separation between PEG and 500 kDa Dextran (Sigma-Aldrich). During the fabrication process, microparticles were labeled with AlexaFluor-568 (Sigma-Aldrich). The microparticles used in this work were 85 µm in diameter, with an inner cavity diameter of 60 µm.

*DNA oligos and target sequences*: λ phage DNA was purchased from Thermo Fisher Scientific (Waltham, MA, USA). All primers were ordered through Invitrogen Custom Oligos (Carlsbad, CA, USA). Primer sequences are available in **Supplemental Table 1.1**.

*PCR reagents*: Reactions were prepared using 2x Digital PCR Evagreen Supermix (Bio-Rad, Hercules, CA, USA) with 0.01 U/µL added Taq Polymerase (Thermo-Fisher, Waltham, MA, USA). 250 nM forward and reverse primer were added, as well as DNA targets at varying concentrations.

*Microparticle encapsulation and emulsification*: Microparticle pellet (in 0.1% Pluronic) was added to each PCR reaction to QS the PCR reagents to proper concentrations. After 10 minutes to allow for mixing, all samples are spun at 9800 x g for 5 minutes. The supernatant was removed via pipetting. Droplet Generation Oil for Evagreen (Bio-Rad, Hercules, CA, USA) was added in double the volume of the microparticle pellet. The oil-particle mixture was then pipetted repeatedly at 60 bpm for 30 seconds followed by 120 bpm for 60 seconds.

*PCR cycling*: Samples were loaded in the Eppendorf Mastercycler Personal (Hamburg, Germany). After an initial denaturation step at 95 °C for 5 minutes, samples were cycled 35 times between 95 °C for 30 seconds and 65 °C for 1 minute. The lid temperature was set to 105 °C to prevent evaporation and coalescence of the emulsions. The temperature cycling information was informed by the recommended PCR protocol from the Bio-Rad 2x Digital PCR Evagreen Supermix.

*Fluorescent Microscope Imaging*: Fluorescent microscope images were obtained using the Nikon Eclipse TI Microscope (Melville, NY, USA). Multi-channel images were obtained of the microparticles in emulsion at 1 second exposure in the FITC channel (495/519 nm excitation/emission) and 500 ms exposure in the TRITC channel (544/570 nm). Images were

analyzed for fluorescence intensity using a custom MATLAB script (available from Gitlab upon request).

**Results**

We demonstrate a dPCR workflow that was accomplished using only common laboratory equipment: consisting of micropipettes, a benchtop centrifuge, and a fluorescence microscope. The workflow and required laboratory equipment for cavitary microparticle dPCR is demonstrated in **Figure 2.1**. PCR reagents were first prepared as normal, then a densely packed pellet of microparticles was added to each reaction tube, as shown in **Figure 2.1a**. The same tools common to PCR reaction preparation, a benchtop centrifuge and a micropipette, were then used to form the reaction partitions for dPCR. Upon concentrating the microparticles through centrifugation and removing the supernatant, droplet generation oil was added, and the mixture was repeatedly aspirated with a micropipette. The shear induced by passing in and out of the pipette tip yielded water-in-oil emulsions, as shown in **Figure 2.1b**.

While emulsification via pipetting generated droplets of various sizes, the emulsions formed around the hydrogel microparticles are templated by the exterior surface of the particle to yield partitions of similar volume. A section of the microparticle interior was shielded from polymerization during aqueous two phase separation fabrication process[72]. The resultant cavity within the microparticle templated emulsion enables more space for large macromolecules, such as template DNA and polymerase, to exist without exclusion by the dense microparticle matrix, as illustrated in **Figure 2.2a**.

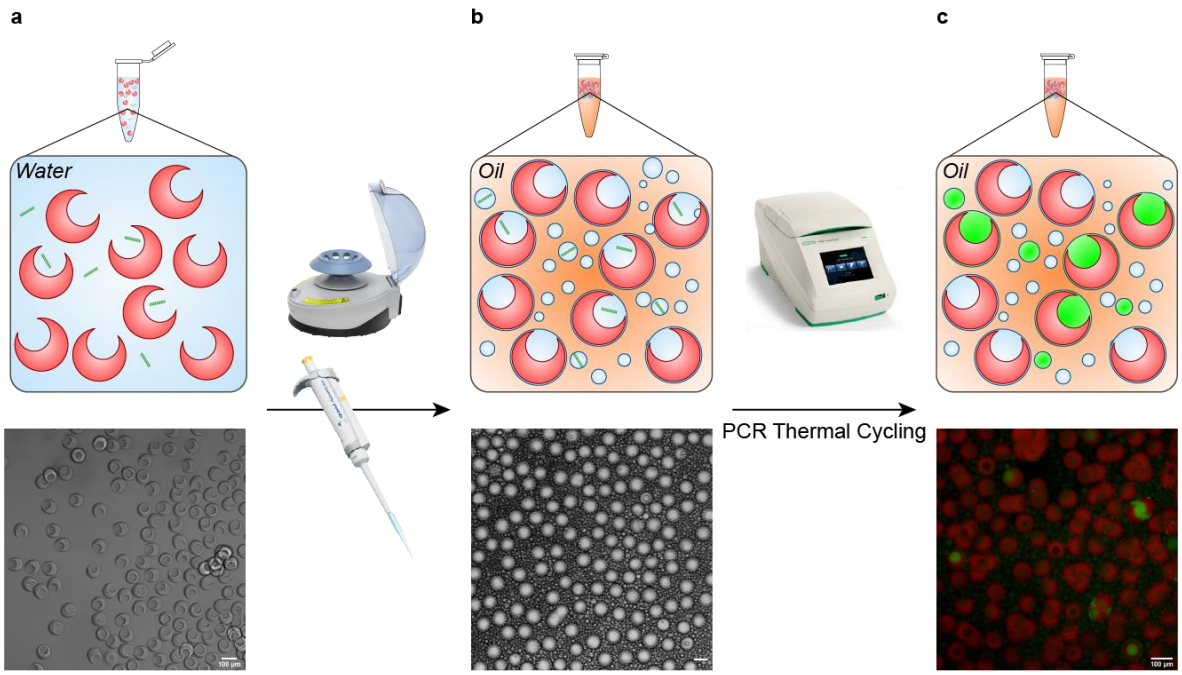


***Figure 2.1: Digital PCR Assay Accomplished Using Common Laboratory Equipment.*** *Strategy for performing dPCR with readily accessible research tools with representative micrographs for each workflow step.* ***A.*** *Hydrogel microparticles are added to PCR reagents, where single entities of DNA are captured inside of the microparticle cavity. Samples are then spun down with a benchtop centrifuge, supernatant aspirated, and oil added on top of the sample.* ***B.*** *Pipetting the oil and water mixture results in the formation of water-in-oil emulsions, with uniform aqueous partition volumes forming around the hydrogel microparticles. Emulsions without microparticles, referred to as satellite drops, will also form during emulsification, but these partitions can be ignored through fluorescent labeling of the microparticles and imaging via fluorescence microscopy.* ***C.*** *Emulsified samples are placed in a standard PCR thermal cycler to amplify the DNA in the reaction partitions that contain a DNA entity. Fluorescent intercalating*

*dye increases quantum yield in the presence of DNA, therefore indicating the presence of a DNA entity upon bright fluorescent signal in that partition. Scale bars shown are 100 µm.*

We further characterized the hydrogel exclusion of macromolecules for both spherical and cavitary microparticles using the inert fluorophore fluorescein isothiocyanate (FITC). To characterize the aqueous volume available to large macromolecular PCR reagents, we utilized FITC conjugated to high molecular weight Dextran. The molecular weight of the utilized FITC-Dextran, 500 kDa, was informed by the molecular weight cutoff of our hydrogel matrix, which we observed to be approximately 100 kDa (unpublished data). Fluorescence micrographs demonstrate the exclusion of FITC-Dextran by the hydrogel matrix, shown in **Figure 2.2b**. The bright fluorescent signal in the cavity of the cavitary microparticles indicates further volume available for macromolecules in contrast to spherical microparticles. This additional aqueous volume further improves the Poisson loading characteristics of the cavitary microparticle partitions, for which calculations are shown in **Supplemental Table 2.2**.

Upon emulsion formation, the dPCR samples were thermal cycled using a standard PCR thermal cycler. The PCR master mix utilized was pre-loaded with the fluorescent intercalating dye Evagreen to indicate the presence of amplification, as illustrated in **Figure 2.1c**. Emulsions containing target DNA underwent amplification during thermal cycling, upon which Evagreen molecules bound to the polymerized DNA and elicited bright fluorescent signal upon excitation with blue light.

After thermal cycling , the emulsions were loaded into a PDMS reservoir and imaged using fluorescence microscopy. To distinguish emulsions in microparticles from satellite droplet emulsions, the microparticles were fluorescently labeled in a different channel than that of Evagreen. Representative multi-channel fluorescence images are shown in **Figure 2.3a**. Bright

fluorescent signal was observed in several partitions when target DNA was added to the PCR sample. Minimal positive partitions were observed in the negative template control samples.

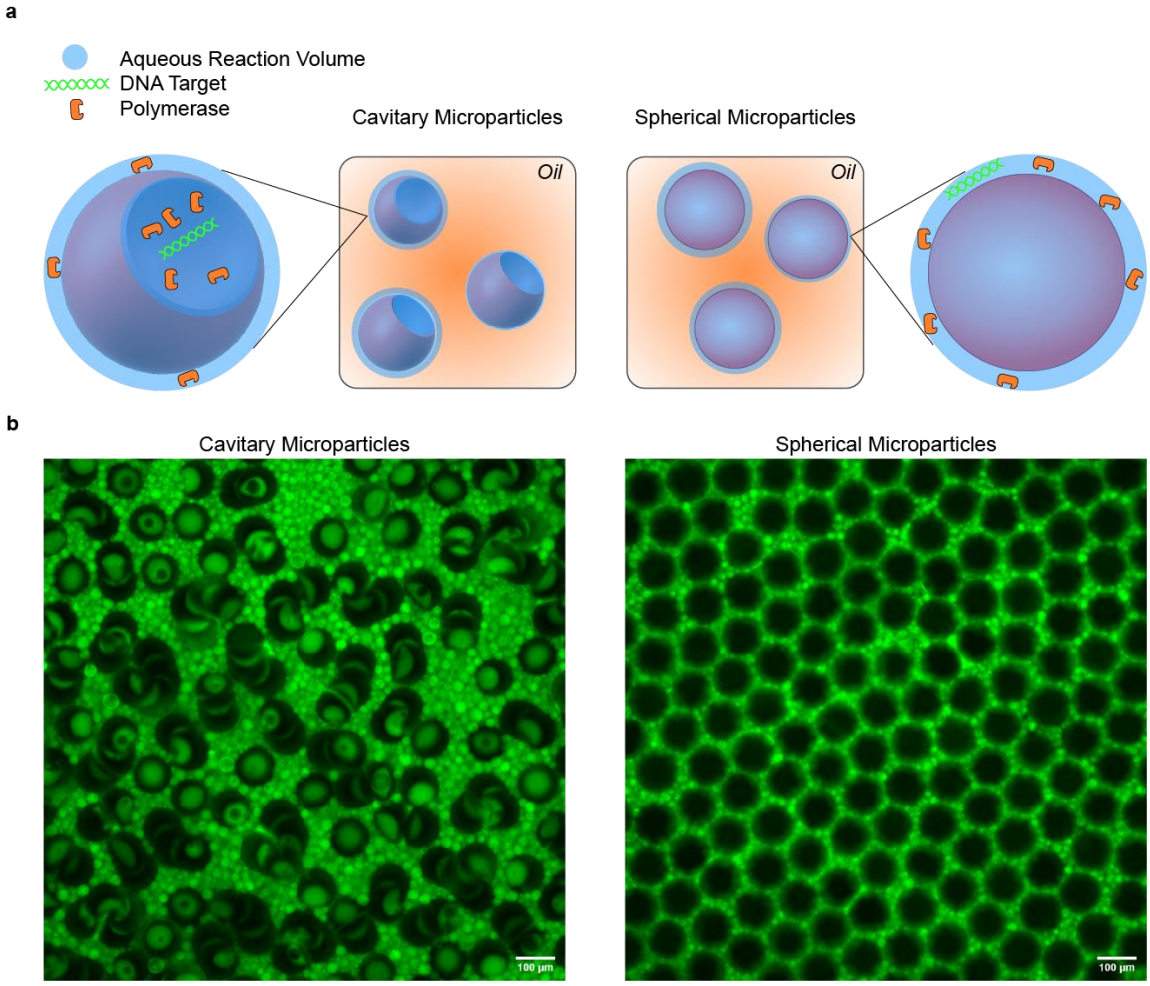


***Figure 2.2: Cavitary Microparticle Geometry Increases Reaction Volume Amenable to PCR Macromolecules. A.*** *Three-dimensional rendering of cavitary and spherical microparticle templated emulsions in oil. The open cavitary geometry further increases the volume accessible to large macromolecules such as template DNA and polymerase, as these molecules are unable to diffuse through the microparticle polymer matrix.* ***B.*** *Fluorescence micrographs of cavitary microparticles and spherical microparticles in emulsions with 0.5 µM FITC-Dextran 500 kDa. Hydrogel matrix exclusion of the large molecule fluorophore indicates exclusion of macromolecular PCR reagents of similar size. Scale bars shown are 100 µm.*

Targeting λ phage DNA as proof of concept, we tested our dPCR platform at two different DNA concentrations. Using the Poisson loading model, we calculated that the lower of the two sample DNA concentrations theoretically yielded predominately 0 or 1 entities per partition, and that of the higher of the two concentrations theoretically yielded 1 or more entities in nearly every partition, for which calculations are shown in **Supplemental Table 2.2**. Both calculated Poisson loading coefficients are common for validating digital PCR assays and have been shown to be within the range upon which digital PCR is the most precise based on Poisson loading models[69,73].

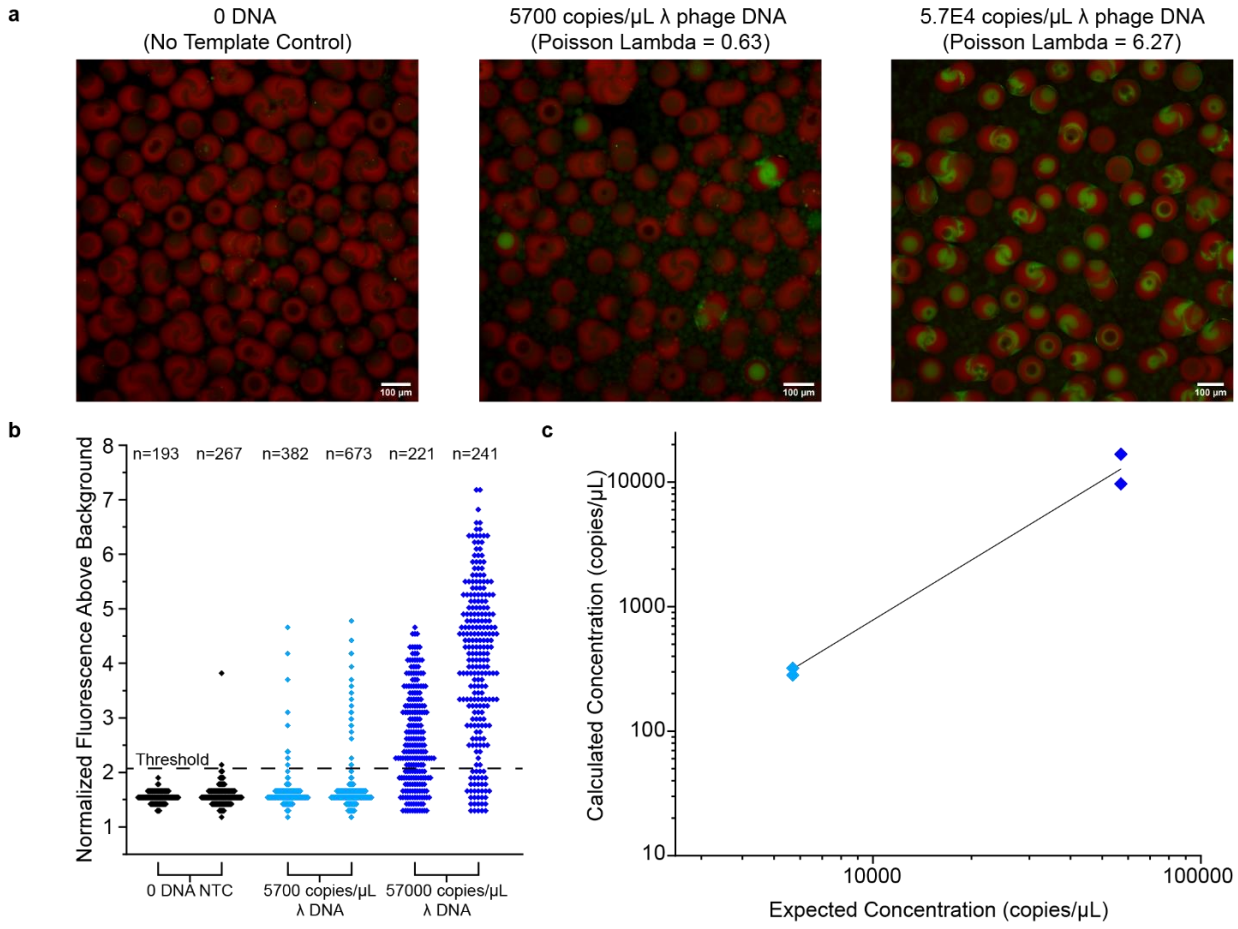


***Figure 2.3: Digital PCR in Cavitary Microparticle Templated Emulsions. A.*** *Representative multi-channel fluorescence micrographs of digital PCR samples after amplification. As DNA*

*concentration increases, more microparticles exhibit high fluorescent signal in the FITC channel, indicating increased fluorescence of Evagreen, a DNA intercalating dye whose intensity correlates to presence of DNA. Poisson loading coefficients compare the starting sample DNA concentration to the probability of a partition holding a DNA entity. Micrograph lookup tables were adjusted for image uniformity and ease of viewing. Scale bar shown is 100 µm.* ***B.*** *Dot plots of fluorescence intensity for digital PCR samples at various DNA concentrations. Threshold line indicates 99% confidence threshold calculated from the collated NTC conditions. Bin size shown indicates the bin size utilized in the negative template controls to calculate the positivity threshold.* ***C.*** *Comparison of loaded DNA sample concentration to the concentration calculated via Poisson loading with illustrative quantification trendline. Disparity between calculated and expected concentrations indicate a concentration quantification inaccuracy of approximately one order of magnitude. N = 2 for both concentrations.*

Microscope images of the cavitary microparticles were then analyzed using a custom MATLAB script. After detecting the cavitary microparticles in the microparticle label fluorescence channel (TRITC), the interior of each microparticle was sampled for pixel intensity in the Evagreen channel (FITC). Partitions that were considered "positive" had fluorescence values above the 99% confidence threshold calculated from the negative template control samples, a common fluorescence threshold parameter[74,75]. **Figure 2.3b** shows the increase in microparticles with fluorescence values above the set threshold as DNA concentration increases. We confirmed the validity of the 99% confidence threshold using the Kolmogorov-Smirnov test ($p<0.01$) to confirm our negative template controls were normally distributed. **Supplemental Figure 2.1** shows the 99% confidence threshold as calculated from the set of collated negative template controls.

***Table 2.1: Calculated DNA Concentration Accuracy in Cavitary Microparticle Digital PCR.***

*Ratio of calculated concentration via Poisson loading to expected DNA concentration of known stock solution of λ phage DNA. The averaged quantitative inefficiency was 14%, indicating slightly under an order of magnitude loss between calculated and expected DNA concentration.*

| Expected DNA Concentration (copies/µL) | Calculated DNA Concentration 1 (copies/µL) | Quantitative Inefficiency (ratio) | Calculated DNA Concentration 2 (copies/µL) | Quantitative Inefficiency (ratio) |
|---|---|---|---|---|
| 5700 | 282 | 5% | 321 | 6% |
| 57000 | 9674 | 17% | 16811 | 29% |

From the number of positive reaction partitions, we calculated the DNA concentration in each sample using the Poisson loading formula. Calculated concentrations are shown in **Figure 2.2C**, which indicate a disparity from the expected DNA concentration loaded in the sample. **Table 2.1** shows each calculated quantitative inefficiency ratio as well as the averaged inefficiency ratio between calculated and expected DNA concentrations from each sample. The quantification inaccuracy of calculated DNA concentration was approximately one order of magnitude below the expected absolute concentration of a sample. Each quantitative inefficiency was calculated as:

$$\text{Quantitative Inefficiency} = \frac{\text{Calculated DNA Concentration}}{\text{Expected DNA Concentration}}$$

**Discussion**

The data shown herein preliminarily demonstrates the advantages of cavitary microparticles over spherical microparticles for digital PCR. Immediate further work to confirm these advantages include comparing assay precision and accuracy to that of dPCR performed in spherical microparticle templated emulsions. We expect an even greater assay quantitative inefficiency in dPCR with spherical microparticles than the inaccuracies shown in **Table 2.1**

with cavitary microparticles, as volume fluctuations are known to detrimentally affect PCR efficiency[71].

Cavitary microparticle geometry yields an increase in volume available to macromolecular PCR reagents, and therefore may improve the quantitative efficiency of dPCR in cavitary microparticle emulsions over that of spherical microparticles. Other small molecules common to PCR, such as salts, nucleotides, and intercalating dyes, have been theorized to freely diffuse through the matrix of hydrogels similar in composition to the hydrogel microparticles we used[67]. However, if the large macromolecular reagents are excluded from these regions by the dense hydrogel matrix, those small molecules cannot be accessed by the large macromolecules to polymerize new DNA. Upon comparison of dPCR quantitative efficiency of spherical microparticles to that of the cavitary microparticles shown here, improved volume available to macromolecules in cavitary microparticles may explain an improved reaction efficiency over that of spherical microparticles.

The theorized improvement in dPCR quantitative accuracy may also be a result of more uniformized partition volumes through the cavitary geometry of the microparticles we used. The thin aqueous volume between emulsion diameter and microparticle diameter may induce greater reaction volume variability in spherical microparticles. This effect is likely reduced in the cavitary microparticles, as the volume of the interior cavity is not impacted by the emulsion interface.

The ease of use and minimal equipment requirements of microparticle partition generation greatly improve access to dPCR in comparison to established dPCR systems. Most conventional dPCR platforms, particularly those commercially available, require specialized and often expensive equipment for partition generation and amplification readout[65]. As dPCR is also

known to have better overall quantitative capabilities than that of rtPCR, the increased accessibility of microparticle-based dPCR systems may increase the prevalence of dPCR applications in fields such as point-of-care diagnostics[62]. Isothermal amplification reactions such as Loop Mediated Isothermal Amplification (LAMP), which are more amenable to resource limited settings than PCR thermal cycling, warrant further investigation in microparticle-based digital assays to increase the point-of-care applicability of digital nucleic acid amplification[47,76].

Assay optimization may further improve the precision and accuracy in quantifying sample DNA concentration in dPCR. The observed quantification inefficiency of approximately one order of magnitude in our dPCR assay currently detrimentally affects our assay sensitivity and limit of detection. However, we observed that quantification inaccuracy is reduced at higher DNA concentrations, as shown in **Table 2.1**. This is likely a result of multiple entity loading per partition based on Poisson calculations, as shown in **Supplemental Table 2.2**. Adding reagents such as Bovine Serum Albumin and dye sequestering agents may further improve reaction efficiency and enable more accurate quantification of target DNA[38,77].

Highly sensitive readout methods may additionally improve dPCR quantification accuracy. Devices with photomultiplier detectors may achieve more sensitive detection and greater signal-to-noise ratio than fluorescence microscopy. Greater signal-to-noise may improve determination of partitions above the positivity threshold, furthering the quantitative inefficiency. Emulsion compatible platforms such as the On-Chip sorter present promising implementation opportunities for future microparticle dPCR readout[78].

Dynamic range and limit of detection may be further improved by the versatility of aqueous two-phase separation for controlling microparticle geometries. Adjusting the concentrations of the two polymer-precursor phases during fabrication yields various sizes of

microparticle cavities[72]. As Poisson loading is dependent on partition volume, shown in **Supplemental Table 2.2**, the cavity size of microparticles can be optimized for Poisson loading at an expected DNA concentration. Combining microparticles of different cavity size may further increase assay dynamic range, where larger microparticles improve Poisson loading at low concentrations of DNA, and smaller microparticles improve Poisson loading for high concentrations.

The solid substrate of microparticle surfaces enables PCR product capture through conjugation of oligonucleotides to microparticles. Product conjugation to the microparticles may enable amplification detection in aqueous phase, with emulsions being broken after the reaction is complete. Detection in aqueous phase may improve compatibility of microparticle dPCR with high throughput readout methods such as flow cytometry. PCR product capture has been demonstrated previously through BEAMing, where PCR product was annealed to complementary oligonucleotides on the surface of spherical microparticles[68]. Oligonucleotide barcoding of particles with different cavity sizes may enable dPCR multiplexing while tuning each partition volume to the expected concentrations of each target. Further advances in microparticle fabrication, including shape barcoding, present further opportunities for advancing PCR multiplexing past the limits of conventional fluorescence-channel based multiplexing[79,80].

**Conclusion**

We demonstrate preliminary data toward achieving democratized microparticle dPCR through cavitary microparticle geometry. Eliminating microfluidic partition generation platforms greatly improves the accessibility to digital platforms for laboratories currently using analog assays. Previous studies have highlighted the high sensitivity of digital assays to several reaction parameters[48]. The increased access to digital platforms in research settings through use of

cavitary microparticles may increase the prevalence of studies further optimizing these parameters. Cavitary microparticle partition formation may also be applied to other single molecule assays, such as digital ELISA. Future reagent and platform optimization will further improve the quantitative accuracy of microparticle-based digital assays, which may ultimately foster the achievement of microparticle-based digital assay capabilities comparable to that of current commercial systems.

**Appendix B: Supplemental Information for Chapter 2**

***Supplemental Table 2.1: Primer sequences for* λ phage DNA**. *All sequences are provided in 5' to 3' orientation.*

| | |
|---|---|
| FIP | **CAGCCAGCCGCAGCACGTTCGCTCATAGGAGATATGGTAGAGCCGC** |
| BIP | **GAGAGAATTTGTACCACCTCCCACCGGGCACATAGCAGTCCTAGGGACAGT** |
| F3 | **GGCTTGGCTCTGCTAACACGTT** |
| B3 | **GGACGTTTGTAATGTCCGCTCC** |
| LoopF | **CTGCATACGACGTGTCT** |
| LoopB | **ACCATCTATGACTGTACGCC** |

***Supplemental Table 2.2: Poisson Loading for λ Phage DNA in Cavitary Microparticles.***

*Calculations of the theoretical Poisson Lambda Coefficient for varying sample concentrations of DNA. Theoretical ratio of empty microparticles to those with at least one DNA entity informed the chosen concentrations for samples accounting for inefficiencies.*

| DNA Sample Concentration (copies/μL) | Partition Volume (μL/partition) | Theoretical Loading Coefficient (λ) | Theoretical Empty Partitions ($x = 0$) | One DNA Entity ($x = 1$) | Two or more entities ($x > 2$) |
|---|---|---|---|---|---|
| 5700 | 1.13E-4 | 0.627 | 52% | 33% | 13% |
| 57000 | 1.13E-4 | 6.27 | 0.1% | 1% | 98% |

Upon consideration of the partitions to be primarily comprised of the volume of the inner cavity, thus considering the thin microparticle-emulsion shell volume as negligible, we calculated the partition volume as:

$$V_{partition} = \frac{4\pi}{3}\left(r_{cavity}\right)^3$$

Treating each copy of DNA as a single entity of interested, we calculated the Theoretical Loading Coefficient in entities per partition:

$$\lambda = \text{concentration}\left(\frac{\text{entities}}{\mu\text{L}}\right) \times \text{partition volume}\left(\frac{\mu\text{L}}{\text{partition}}\right) = \text{loading coefficient}\left(\frac{\text{entities}}{\text{partition}}\right)$$

The fraction of partitions containing a certain number of entities *x* was then calculated at each λ using the Poisson Distribution formula:

$$P(X = \text{x}) = \frac{\lambda^x}{x!}e^{-\lambda}$$

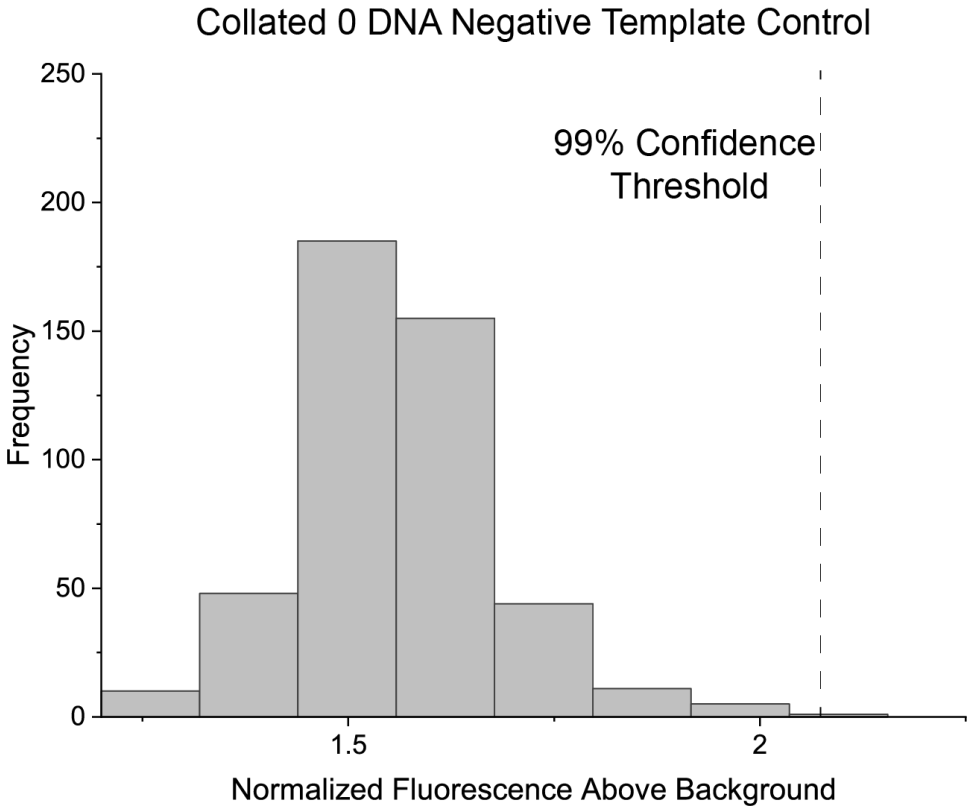


***Supplemental Figure 2.1: Determination of Positive Threshold via Distribution Calculation of Negative Template Controls.*** *Histogram of fluorescence frequency distribution with bin size of 0.119. Upon calculation of the cumulative distribution function $S_n(x)$, the confidence threshold was set to the value at which $S_n(x)$ is greater than 99%, with z-score of 3.82. N=459 partitions.*

## References


1. Jones, P. A. & Baylin, S. B. The fundamental role of epigenetic events in cancer. *Nat. Rev. Genet.* **3**, 415–428 (2002).
2. Robertson, K. D. DNA methylation and human disease. *Nat. Rev. Genet.* **6**, 597 (2005).
3. Dor, Y. & Cedar, H. Principles of DNA methylation and their implications for biology and medicine. *Lancet* **392**, 777–786 (2018).
4. Webster, A. L. H., Yan, M. S. & Marsden, P. A. Epigenetics and Cardiovascular Disease. *CJCA* **29**, 46–57 (2013).
5. Das, P. M. & Singal, R. DNA methylation and cancer. *J. Clin. Oncol.* **22**, 4632–4642 (2004).
6. Shen, S. Y. *et al.* Sensitive tumour detection and classification using plasma cell-free DNA methylomes. *Nature* **563**, 579–583 (2018).
7. Nguyen, A., Mamarbachi, M., Turcot, V., Lessard, S. & Yu, C. Lower Methylation of the ANGPTL2 Gene in Leukocytes from Post-Acute Coronary Syndrome Patients. 1–17 (2016) doi:10.1371/journal.pone.0153920.
8. Lund, G. & Zaina, S. Atherosclerosis: An epigenetic balancing act that goes wrong. *Current Atherosclerosis Reports* vol. 13 208–214 (2011).
9. Post, W. S. *et al. Methylation of the estrogen receptor gene is associated with aging and atherosclerosis in the cardiovascular system*. *Cardiovascular Research* vol. 43 www.elsevier.com/locate/cardioreswww.elsevier.nl/locate/cardiores (1999).
10. Zhou, J. *et al.* Preliminary study of the relationship between promoter methylation of the ANGPTL2 gene and coronary heart disease. *J. Clin. Lab. Anal.* **33**, 1–7 (2019).
11. Oxnard, G. R. *et al.* Prognostic significance of blood-based cancer detection in plasma

cell-free DNA (cfDNA): Evaluating risk of overdiagnosis. *J. Clin. Oncol.* **37**, 1545–1545 (2019).

12. Oxnard, G. R. *et al.* Simultaneous multi-cancer detection and tissue of origin (TOO) localization using targeted bisulfite sequencing of plasma cell-free DNA (cfDNA). *Ann. Oncol.* **30**, v912 (2019).
13. Ofman, J. J., Hall, M. P., Aravanis, A. & GRAIL inc. GRAIL and the quest for earlier multi-cancer detection. https://www.nature.com/articles/d42473-020-00079-y.
14. Craw, P. & Balachandran, W. Isothermal nucleic acid amplification technologies for point-of-care diagnostics : a critical review. *Lab Chip* **12**, 2469–2486 (2012).
15. St John, A. & Price, C. P. Existing and Emerging Technologies for Point-of-Care Testing. *Clin. Biochem. Rev.* **35**, 155–167 (2014).
16. Ahluwalia, N. *et al.* Prognostic value of multiple emerging biomarkers in cardiovascular risk prediction in patients with stable cardiovascular disease. *Atherosclerosis* **228**, 478–484 (2013).
17. Finegold, J. A., Asaria, P. & Francis, D. P. Mortality from ischaemic heart disease by country, region, and age: Statistics from World Health Organisation and United Nations. *Int. J. Cardiol.* **168**, 934–945 (2013).
18. Baccarelli, A. A. & Byun, H. M. Platelet mitochondrial DNA methylation: A potential new marker of cardiovascular disease. *Clin. Epigenetics* **7**, 1–9 (2015).
19. Yang, Q., Zhao, Y., Zhang, Z. & Chen, J. Association of interleukin-6 methylation in leukocyte DNA with serum level and the risk of ischemic heart disease. *Scand. J. Clin. Lab. Invest.* **76**, 291–295 (2016).
20. Ogino, S. *et al.* Precision and performance characteristics of bisulfite conversion and real-

time PCR (MethyLight) for quantitative DNA methylation analysis. *J. Mol. Diagnostics* **8**, 209–217 (2006).

21. Yi, S., Long, F., Cheng, J. & Huang, D. An optimized rapid bisulfite conversion method with high recovery of cell-free DNA. *BMC Mol. Biol.* **18**, 1–8 (2017).

22. Niemz, A., Ferguson, T. M. & Boyle, D. S. Point-of-care nucleic acid testing for infectious diseases. *Trends Biotechnol.* **29**, 240–250 (2011).

23. Vashist, S. K., Luppa, P. B., Yeo, L. Y., Ozcan, A. & Luong, J. H. T. Emerging Technologies for Next-Generation Point-of-Care Testing. *Trends Biotechnol.* **33**, 692–705 (2015).

24. Herman, J. G., Graff, J. R., Myohanen, S., Nelkin, B. D. & Baylin, S. B. Methylation-specific PCR : A novel PCR assay for methylation status of CpG islands. **93**, 9821–9826 (1996).

25. Nishigaki, K., Kaneko, Y., Wakuda, H., Husimi, Y. & Tanaka, T. Type II restriction endonucleases cleave single-stranded DNAs in general. *Nucleic Acids Res.* **13**, 5747–5760 (1985).

26. Hashimoto, K., Kokubun, S., Itoi, E. & Roach, H. I. Improved quantification of DNA methylation using methylation-sensitive restriction enzymes and real-time PCR. *Epigenetics* **2**, 86–91 (2007).

27. Sehouli, J. *et al.* Epigenetic quantification of tumor-infiltrating T-lymphocytes. *Epigenetics* **6**, 236–246 (2011).

28. Notomi, T. *et al.* Loop-mediated isothermal amplification of DNA. *Nucleic Acids Res.* **28**, e63 (2000).

29. Nagamine, K., Hase, T. & Notomi, T. Accelerated reaction by loop-mediated isothermal

amplification using loop primers. *Mol. Cell. Probes* **16**, 223–229 (2002).

30. Mori, Y., Kitao, M., Tomita, N. & Notomi, T. Real-time turbidimetry of LAMP reaction for quantifying template DNA. *J. Biochem. Biophys. Methods* **59**, 145–157 (2004).

31. Rolando, J. C., Jue, E., Schoepp, N. G. & Ismagilov, R. F. Real-Time, Digital LAMP with Commercial Microfluidic Chips Reveals the Interplay of Efficiency, Speed, and Background Amplification as a Function of Reaction Temperature and Time. *Anal. Chem.* **91**, 1034–1042 (2019).

32. Patel, J. C. *et al.* Field evaluation of a real-time fluorescence loop-mediated isothermal amplification assay, realamp, for the diagnosis of Malaria in Thailand and India. *J. Infect. Dis.* **210**, 1180–1187 (2014).

33. Njiru, Z. K. Loop-mediated isothermal amplification technology: Towards point of care diagnostics. *PLoS Negl. Trop. Dis.* **6**, 1–4 (2012).

34. Zhang, X., Lowe, S. B. & Gooding, J. J. Brief review of monitoring methods for loop-mediated isothermal amplification (LAMP). *Biosens. Bioelectron.* **61**, 491–499 (2014).

35. Zerilli, F. *et al.* Methylation-specific loop-mediated isothermal amplification for detecting hypermethylated DNA in simplex and multiplex formats. *Clin. Chem.* **56**, 1287–1296 (2010).

36. Stefansson, O. A., Villanueva, A., Vidal, A., Martí, L. & Esteller, M. BRCA1 epigenetic inactivation predicts sensitivity to platinum-based chemotherapy in breast and ovarian cancer. *Epigenetics* **7**, 1225–1229 (2012).

37. Mao, F., Leung, W. Y. & Xin, X. Characterization of EvaGreen and the implication of its physicochemical properties for qPCR applications. *BMC Biotechnol.* **7**, 1–16 (2007).

38. Kong, J. E. *et al.* Highly Stable and Sensitive Nucleic Acid Amplification and Cell-Phone-

Based Readout. *ACS Nano* **11**, 2934–2943 (2017).

39. Dhaliwal, A. DNA Extraction and Purification. *Mater. Methods* **3**, 191 (2013).

40. Claassen, S. *et al.* A comparison of the efficiency of five different commercial DNA extraction kits for extraction of DNA from faecal samples. *J. Microbiol. Methods* **94**, 103–110 (2013).

41. Spiess, A. N., Feig, C. & Ritz, C. Highly accurate sigmoidal fitting of real-time PCR data by introducing a parameter for asymmetry. *BMC Bioinformatics* **9**, 221 (2008).

42. Price, R. J., Lillycrop, K. A. & Burdge, G. C. Folic acid supplementation in vitro induces cell type-specific changes in BRCA1 and BRCA 2 mRNA expression, but does not alter DNA methylation of their promoters or DNA repair. *Nutr. Res.* **35**, 532–544 (2014).

43. Xu, J. *et al.* CpG island methylation affects accessibility of the proximal BRCA1 promoter to transcription factors. *Breast Cancer Res. Treat.* **120**, 593–601 (2010).

44. Marimuthu, K., Jing, C. & Chakrabarti, R. Sequence-Dependent Biophysical Modeling of DNA Amplification. *Biophys. J.* **107**, 1731–1743 (2014).

45. Agostini, H. T. & Stoner, G. L. Amplification of the complete polyomavirus JC genome from brain, cerebrospinal fluid and urine using pre-PCR restriction enzyme digestion. *J. Neurovirol.* **1**, 316–320 (1995).

46. Shiraishi, M. & Hayatsu, H. *High-Speed Conversion of Cytosine to Uracil in Bisulfite Genomic Sequencing Analysis of DNA Methylation*. *DNA Research* vol. 11 https://academic.oup.com/dnaresearch/article-abstract/11/6/409/368140 (2004).

47. Rolando, J. C., Jue, E., Barlow, J. T. & Ismagilov, R. F. Real-time kinetics and high-resolution melt curves in single-molecule digital LAMP to differentiate and study specific and non-specific amplification. *Nucleic Acids Res.* **48**, e42 (2020).

48. Rolando, J. C., Jue, E., Schoepp, N. G. & Ismagilov, R. F. Real-Time, Digital LAMP with Commercial Microfluidic Chips Reveals the Interplay of Efficiency, Speed, and Background Amplification as a Function of Reaction Temperature and Time. *Anal. Chem.* **91**, 1034–1042 (2019).

49. Wu, Z. *et al.* Absolute quantification of DNA methylation using microfluidic chip-based digital PCR. *Biosens. Bioelectron.* **96**, 339–344 (2017).

50. Kuspa, A. & Loomis, W. F. *Tagging developmental genes in Dictyostelium by restriction enzyme-mediated integration of plasmid DNA (transformation/insertional mutageneis/gene cloning)*. *Genetics* vol. 89 (1992).

51. Muñoz, H. E. *et al.* Fractal LAMP: Label-Free Analysis of Fractal Precipitate for Digital Loop-Mediated Isothermal Nucleic Acid Amplification. *ACS Sensors* **5**, 385–394 (2020).

52. Hu, Y., Xu, P., Luo, J., He, H. & Du, W. Absolute Quantification of H5-Subtype Avian Influenza Viruses Using Droplet Digital Loop-Mediated Isothermal Amplification. (2016) doi:10.1021/acs.analchem.6b03328.

53. Kint, S., De Spiegelaere, W., De Kesel, J., Vandekerckhove, L. & Van Criekinge, W. Evaluation of bisulfite kits for DNA methylation profiling in terms of DNA fragmentation and DNA recovery using digital PCR. *PLoS One* **13**, e0199091 (2018).

54. Yu, M. *et al.* Methylight droplet digital PCR for detection and absolute quantification of infrequently methylated alleles. *Epigenetics* **10**, 803–809 (2015).

55. Zemmour, H. *et al.* Non-invasive detection of human cardiomyocyte death using methylation patterns of circulating DNA. *Nat. Commun.* **9**, (2018).

56. Dhurat, R. & Sukesh, M. Principles and methods of preparation of platelet-rich plasma: A review and author′s perspective. *J. Cutan. Aesthet. Surg.* **7**, 189 (2014).

57. Born, G. V. R. & Cross, M. J. The aggregation of blood platelets. *J. Physiol.* **168**, 178–195 (1963).

58. Lal, G. *et al.* Epigenetic Regulation of Foxp3 Expression in Regulatory T Cells by DNA Methylation. *J. Immunol.* **182**, 259–273 (2009).

59. Basu, A. S. Digital Assays Part I: Partitioning Statistics and Digital PCR. *SLAS Technol.* **22**, 369–386 (2017).

60. Taylor, S. C., Laperriere, G. & Germain, H. Droplet Digital PCR versus qPCR for gene expression analysis with low abundant targets: From variable nonsense to publication quality data. *Sci. Rep.* **7**, 1–8 (2017).

61. Hindson, B. J. *et al.* High-throughput droplet digital PCR system for absolute quantitation of DNA copy number. *Anal. Chem.* **83**, 8604–8610 (2011).

62. Hindson, C. M. *et al.* Absolute quantification by droplet digital PCR versus analog real-time PCR. *Nat. Methods* **10**, 1003–1005 (2013).

63. Wu, Z. *et al.* Absolute quantification of DNA methylation using microfluidic chip-based digital PCR. *Biosens. Bioelectron.* **96**, 339–344 (2017).

64. Vogelstein, B. & Kinzler, K. W. Digital PCR. *Genetics* **96**, 9236–9241 (1999).

65. Baker, M. Digital PCR hits its stride. *Nat. Methods* **9**, 541–544 (2012).

66. Dong, L. *et al*. Comparison of four digital PCR platforms for accurate quantification of DNA copy number of a certified plasmid DNA reference material. *Nat. Publ. Gr.* **2015**, (2015).

67. Hatori, M. N., Kim, S. C. & Abate, A. R. Particle-Templated Emulsification for Microfluidics-Free Digital Biology. *Anal. Chem.* **90**, 9813–9820 (2018).

68. Diehl, F. *et al.* BEAMing: Single-molecule PCR on microparticles in water-in-oil

emulsions. *Nat. Methods* **3**, 551–559 (2006).

69. Majumdar, N., Banerjee, S., Pallas, M., Wessel, T. & Hegerich, P. Poisson Plus Quantification for Digital PCR Systems. *Sci. Rep.* **7**, 1–10 (2017).

70. Bhat, S., Herrmann, J., Armishaw, P., Corbisier, P. & Emslie, K. R. Single molecule detection in nanofluidic digital array enables accurate measurement of DNA copy number. *Anal. Bioanal. Chem.* **394**, 457–467 (2009).

71. Quan, P.-L., Sauzade, M. & Brouzes, E. dPCR: A Technology Review. *Sensors* **18**, 1271 (2018).

72. De Rutte, J., Dimatteo, R., Van Zee, M., Damoiseaux, R. & Carlo, D. Di. Massively parallel encapsulation of single cells with structured microparticles and secretion-based flow sorting. *bioRxiv* (2020) doi:10.1101/2020.03.09.984245.

73. Shen, F., Du, W., Kreutz, J. E., Fok, A. & Ismagilov, R. F. Digital PCR on a SlipChip. *Lab Chip* **10**, 2666–2672 (2010).

74. Strain, M. C. *et al.* Highly Precise Measurement of HIV DNA by Droplet Digital PCR. *PLoS One* **8**, e55943 (2013).

75. Milbury, C. A. *et al.* Determining lower limits of detection of digital PCR assays for cancer-related gene mutations. *Biomol. Detect. Quantif.* **1**, 8–22 (2014).

76. Chen, J. *et al.* BEAMing LAMP: Single-molecule capture and on-bead isothermal amplification for digital detection of hepatitis C virus in plasma. *Chem. Commun.* **54**, 291–294 (2018).

77. Cao, Y., Raith, M. R. & Griffith, J. F. Droplet digital PCR for simultaneous quantification of general and human-associated fecal indicators for water quality assessment. *Water Res.* **70**, 337–349 (2015).

78. Hasegawa, N. *et al.* Detection of circulating sarcoma tumor cells using a microfluidic chip-type cell sorter. *Sci. Rep.* **9**, 1–8 (2019).

79. Kamau, E., Alemayehu, S., Feghali, K. C., Saunders, D. & Ockenhouse, C. F. Multiplex qPCR for Detection and Absolute Quantification of Malaria. *PLoS One* **8**, e71539 (2013).

80. Destgeer, G., Ouyang, M., Wu, C.-Y. & Di Carlo, D. Fabrication of 3D concentric amphiphilic microparticles to form uniform nanoliter reaction volumes for amplified affinity assays. *Lab Chip* **20**, 3503 (2020).